Coupled parametric oscillators: From disorder-induced current to asymmetric Ising model

C. Han,[1,2] M. Wang,[1,2] B. Zhang,[1,2] M. I. Dykman,[3,*] and H. B. Chan[1,2,†]

[1]*Department of Physics, The Hong Kong University of Science and Technology, Clear Water Bay, Kowloon, Hong Kong, China*

[2]*William Mong Institute of Nano Science and Technology, The Hong Kong University of Science and Technology, Clear Water Bay, Kowloon, Hong Kong, China*

[3]*Department of Physics and Astronomy, Michigan State University, East Lansing, Michigan 48824, USA*

(Received 6 December 2023; accepted 23 April 2024; published 13 May 2024)

We study the effects of the interplay of weak disorder and weak coupling in a system of parametric micromechanical oscillators. Each oscillator is bistable, enabling the mapping of its stable states onto spin states. The coupling changes the rate of interstate switching of an oscillator depending on the state of other oscillators. We demonstrate that the change is exponentially strong and therefore manifests even for weak coupling. Difference in the oscillator eigenfrequencies translates into disorder in the system. The analysis and the experiment show that disorder leads to a nontrivial stationary state that displays current. The system provides a well-controlled and fully characterized implementation of the asymmetric Ising model, in which coupled spins affect each other differently. This model plays an important role in physics and biology. Our findings open the possibilities of constructing and exploring asymmetric Ising systems with controlled parameters and connectivity.

DOI: 10.1103/PhysRevResearch.6.023162

I. INTRODUCTION

Parametric oscillator is one of the best-known examples of a bistable system. It has two vibrational states with equal amplitudes and opposite phases [1]. These states emerge when the oscillator eigenfrequency is periodically modulated. They have a period equal to twice the modulation period and can be associated with classical bits or Ising spin states, providing a basis for classical logic operations [2,3]. Superpositions of the opposite-phase coherent states of an oscillator can also encode a qubit [4,5]. Coupled parametric oscillators can serve as Ising machines for classical and quantum annealing [6–14]. Besides computation, various other applications of parametric oscillators have been studied, from force and mass sensing [15,16] to rare events in classical and quantum systems far from thermal equilibrium [17–22] and phase transitions into a time-symmetry-broken (time-crystal) state [23–25].

In many implementations, such as the modes of coupled microwave cavities [26,27], electrical circuits, or mechanical systems [14,25], the individual units in a system of coupled oscillators are not identical. In other words, disorder unavoidably exists. Even weak disorder can have a profound effect on parametric oscillators because their two vibrational states have equal amplitudes and in this sense are degenerate.

An important aspect of Ising systems pointed out by Hopfield [28] is the possibility to use coupled spins to model neural networks, which memorize multiple patterns. This possibility has been attracting increasing interest over the years, particularly in view of the progress in machine learning [29,30]. In the Hopfield model the spin coupling energy has the conventional form of $J_{ij}\sigma_i\sigma_j$, where σ_i, σ_j take on values ± 1 and $J_{ij} = J_{ji}$, and the network dynamics can be analyzed using the methods of statistical physics. The model is symmetric in the sense that the effect of spin i on spin j is the same as the effect of spin j on spin i.

However, most neuron networks are presumably asymmetric: neuron i can affect neuron j stronger than neuron j affects neuron i. If neurons are associated with spins, one can think formally that $J_{ij} \neq J_{ji}$ and then the coupling may not be described by the coupling energy. The corresponding model is called an asymmetric Ising model. It has attracted much attention as one of the leading models of neural networks [31–36] and gene regulatory networks [37] and has been used to describe experiments on neurons (cf. [38,39] and references therein). Overall, the asymmetric Ising model is one of the most important and broadly relevant types of nonreciprocal systems [40].

In spite of the importance of the asymmetric Ising model, there have been no studies that relate the spin coupling parameters to the parameters of the underlying physical system. Understanding the dynamics of this system enables one to examine to what extent the mapping on coupled spins is adequate, in the first place. Determining the relationship between the parameters of the system and the effective spins is essential for implementing and exploring asymmetric Ising models.

In the present paper we demonstrate that, due to the disorder, coupled parametric oscillators provide a system that

*dykmanm@msu.edu
†hochan@ust.hk

can be described by an asymmetric Ising model. Moreover, against common wisdom, we show that disorder, rather than obstructing the current in the system, leads to the onset of a current that circulates in the stationary state. It also leads to nontrivial correlations and nontrivial dynamics that emerge even for nearest-neighbor coupling. The description of our system naturally translates to the Glauber picture [41] in which the rate of switching between the states of a spin depends on the states of the spins to which it is coupled. In the case of oscillators, the relevant quantity is the rate of switching between the period-two vibrational states of an oscillator that depends on which vibrational states are occupied by other oscillators. We describe the mapping of the oscillators on spins and independently measure the parameters of the system that enter the model. In particular, we measure an important characteristic of driven oscillators in the presence of fluctuations, the logarithmic susceptibility [42], which describes the exponentially strong effect of a periodic force on the switching rates of an individual uncoupled parametric oscillator.

The parametric oscillators we study are microelectromechanical resonators modulated close to twice their eigenfrequencies. Such resonators enable exquisite control of their eigenfrequencies and the coupling. Since the decay rates of our resonators are small, the modulation needed to excite parametric vibrations is comparatively weak, so that the vibrations are nearly sinusoidal.

With micromechanical resonators, we demonstrate that the asymmetric Ising model does not have detailed balance. As an immediate consequence, a probability current emerges in the system in the stationary state. We measure this current for a system of two coupled nonidentical parametric oscillators. The measurements are in excellent agreement with the theory.

We consider the case where the coupling of the oscillators is weak, so that each oscillator still has two stable vibrational states, and their amplitudes and phases are only weakly changed by the coupling. However, the coupling can significantly change the rates of noise-induced switching between the states. To gain an intuitive understanding, consider a Brownian particle in a symmetric double-well potential $U(q) = U(-q)$, where q is the particle coordinate. Because of thermal fluctuations, the particle switches between the wells with the rate $W \propto \exp(-\Delta U/k_BT)$, where ΔU is the barrier height and T is temperature [43]. If the potential is tilted, the barrier heights are incremented by $\pm\delta U$ in the opposite wells, breaking the symmetry of the interwell switching rates. The rates acquire extra factors $\exp(\pm\delta U/k_BT)$. Even for a small tilt, the ratio $\delta U/k_BT$ can be large, for low temperatures. In that case the stationary populations of the wells become significantly different.

Consider now a set of weakly interacting particles, each in a double-well potential, with coupling energy $\frac{1}{2}\sum{}'V_{ij}q_iq_j$. A particle localized in a well exerts force on other particles. This force has opposite signs depending on which well the particle occupies. It tilts the potentials of the other particles and breaks the symmetry of their interwell switching rates, see Fig. 1(a).

The key idea here is that, when one particle is switching, which is a rare event, the particles coupled to it are most likely occupying their stable states at the potential minima. One can associate the stable states of individual particles with spin states $\sigma = \pm 1$, and then the interaction

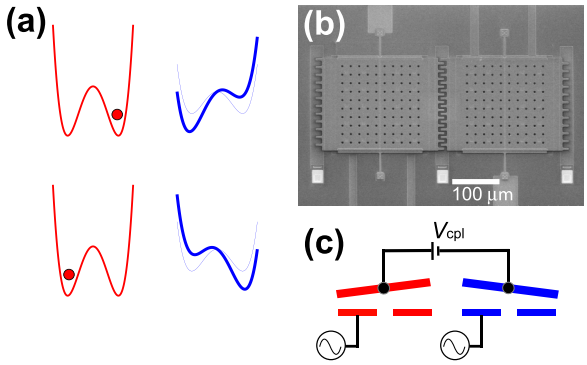

FIG. 1. (a) Two weakly interacting particles in double-well potentials. As shown by the thin-blue lines, the potential of the particle on the right (the "blue" particle) is symmetric in the absence of coupling. When coupling is turned on, this potential is modified depending on the position of the particle on the left (the "red" particle), as represented by the thick-blue lines. It tilts towards the left if the red particle is in the right side of the red potential. In the bottom panel, the red particle is in the left side of the red potential. (b) Scanning electron micrograph of two torsional resonators located side-by-side. The scale bar measures 100 μm. (c) Cross-sectional schematic of the control and actuation scheme. In each resonator, the torsional spring constant is modulated by a periodic voltage on the left electrode to excite parametric resonance, where two vibrational states of the same amplitude but opposite phases coexist. The right electrodes are used to control the eigenfrequencies (Appendix B). The voltage difference V_{cpl} between the top plates controls the capacitive coupling between the two resonators.

between the particles maps onto the spin-spin coupling. The change of the barrier heights and thus the switching rates due to the particle-particle interaction is reminiscent of the spin-spin coupling-induced change of the spin switching rates in the Glauber model. For example, for two coupled spins, the change is $\propto \exp(-\tilde{J}_{12}\sigma_1\sigma_2/k_BT)$ with $\tilde{J}_{12} \propto V_{12}$. Importantly, the two spins affect each other symmetrically even if the potentials of individual particles are different (Appendix A).

As we show, the picture of coupled particles in double-well potentials extends to coupled parametric oscillators, even though there are no static double-well potentials. The extension works if the oscillators are identical and the coupling is weak. In this case the changes of the switching rates are equal within each pair of coupled oscillators. The system is mapped onto the symmetric Ising model. On the other hand, in a qualitative distinction from an equilibrium system of particles in double-well potentials, if the oscillators have different parameters, we show that the coupling-induced changes of the switching rates are different for such oscillators. The picture of a symmetric change in potential barriers no longer applies. Instead, the system is mapped onto the asymmetric Ising model. In our system, switching between the period-two vibrational states is activated by noise with controlled intensity, which allows us to fully characterize the switching rates.

It is important to have an independent way to characterize the effect of the oscillator coupling on the switching rates. We show that it can be done by measuring the change of the switching rates due to an extra drive at half the modulation frequency. We demonstrate that the change of the logarithm of the switching rate is linear in the drive amplitude

and measure the corresponding logarithmic susceptibility. Thus far the logarithmic susceptibility has been only seen in simulations [44].

II. COUPLED MICROMECHANICAL RESONATORS

We present experimental results for a system of two micromechanical torsional resonators. They are shown in Fig. 1(a). Each resonator consists of a movable polysilicon top plate (200 μm × 200 μm × 3.5 μm) supported by two torsional rods, with two fixed electrodes underneath. The resonators are fabricated using a surface micromachining process in which the silicon top plate and electrodes are separated by a 2-μm-thick sacrificial silicon oxide layer. This silicon oxide layer is subsequently etched away so that each top plate is free to rotate about its torsional rod in response to torques applied. The resonators are located side by side. Their vibrations can be excited and detected independently. The vibration eigenfrequencies can be fine-tuned capacitively, including the case where the resonators are coupled, by dc voltages applied to the left and right electrodes (Appendix B). Application of an ac voltage on the left electrode of a resonator generates a periodic electrostatic torque that excites vibrations of the top plate. The vibrations are detected by measuring the current flowing out of the top plate induced by the capacitance change between the plate and the two underlying electrodes.

In this study, only the fundamental modes of torsional vibrations are used. The eigenfrequencies of the resonators are almost identical, with $\omega_1/2\pi \approx 15860.562$ Hz for resonator 1 (the left resonator in Fig. 1) and $\omega_2/2\pi \approx 15860.598$ Hz for resonator 2 (the right resonator in Fig. 1). Long term drifts in $\omega_{1,2}$ are compensated by adjusting the dc voltage on the right electrodes (Appendix B), so that $\omega_{1,2}$ stay within ∼25 mHz of the target values. The damping constants are $\Gamma_1/2\pi \approx 64.2 \pm 0.5$ mHz and $\Gamma_2/2\pi \approx 62.7 \pm 0.3$ mHz for resonators 1 and 2, respectively.

The spring constants of both resonators are modulated electrostatically together at frequency near $2\omega_1 \approx 2\omega_2$, leading to parametric excitation of the vibrations. We also inject independent broadband Gaussian voltage noises for each resonator that lead to occasional switching between the period-two vibrational states.

As shown in Fig. 1(b), the adjacent edges of the plates form interdigitated comb-shaped electrodes to allow the plates to couple when there is a potential difference $V_{\rm cpl}$ between them. When $V_{\rm cpl} = 0$ V, we verify that there is no coupling between the plates. We keep $V_{\rm cpl}$ small as we focus on the regime of the weak coupling that only weakly perturbs the dynamics in the absence of noise.

All measurements are performed at room temperature at pressure below 10 μtorr. The ability to independently tune the eigenfrequencies and the coupling between the resonators is crucial for revealing the features of the asymmetric Ising model.

The equations of motion of coupled parametric oscillators have the form

$$\ddot{q}_i + 2\Gamma_i\dot{q}_i + \omega_i^2 q_i + \gamma_i q_i^3 + M_i^{-1}{\sum_j}' V_{ij}q_j = (F_p/M_i)q_i\cos\omega_p t + \xi_i(t). \quad (1)$$

For our pair of torsional resonators, $i = 1, 2$. The coordinate q_i is the rotation angle of the ith resonator, M_i is its moment of inertia, γ_i is the Duffing nonlinearity parameter, F_p and ω_p are the amplitude and frequency of the parametric modulation, respectively, and $\xi_i(t)$ is zero-mean white Gaussian noise of controlled intensity $4D_i\Gamma_i$, $\langle\xi_i(t)\xi_j(t')\rangle = 4D_i\Gamma_i\delta_{ij}\delta(t-t')$. Parameters V_{ij} are the controlled parameters of the oscillator coupling, with $V_{ij} = V_{ji}$. In the experiments on the effect of the coupling, D_i determines the effective temperature of the noise. We set $D_1 = D_2$.

We use resonant modulation, $|\omega_p - 2\omega_i| \ll \omega_i$, which allows us to parametrically excite vibrations even with small F_p. In the absence of resonator coupling and noise the two stable vibrational states of the ith resonator are

$$q_i(\sigma_i;t) = A_i\sigma_i\cos[(\omega_p/2)t + \varphi_i], \quad (2)$$

where A_i and φ_i are the vibration amplitude and phase, and $\sigma_i = \pm 1$. The values of A_i, φ_i depend on the resonator parameters; for small damping $|\varphi_i| \ll 1$. For brevity, and where it may not cause confusion, we use ↑ and ↓ for $\sigma_i = 1$ and $\sigma_i = -1$, respectively.

In what follows we associate the vibrational states (2) with spin states. This association is justified provided the change of these states because of coupling the oscillators to each other, i.e., the change of the amplitudes A_i and phases φ_i, is small. The weakness of the coupling is thus a major condition of the mapping of the system of oscillators on the system of coupled spins.

A. Interstate switching

Classical and quantum noise causes transitions between the states $\sigma_i = \pm 1$ of an isolated oscillator. By symmetry, the rates $W_i(\sigma_i)$ of transitions $\sigma_i \to -\sigma_i$ of the ith oscillator are the same for the both states. For weak noise, the transitions are rare, $W_i(\sigma_i) \ll \Gamma_i$, and the dependence of the switching rate on the noise intensity is given by the activation law [17,19]. For classical noise

$$W_i(\sigma_i) = C_i\exp[-R_i(\sigma_i)/D_i], \quad (3)$$

where $R_i(\sigma_i) = R_i(-\sigma_i)$ is the effective activation energy and $C_i \propto \Gamma_i$ for weak damping. Activated switching in single parametric oscillators has been measured in a number of systems [18,20,23].

In our experiment, the switching rate of each resonator is extracted from the Poisson distribution of the residence times (Appendix C). Due to slight difference in the damping constants, the switching rates for the two resonators are measured to be different. We verify that, when the coupling is zero, the two coexisting states with opposite phases are equally occupied in each resonator and the populations of all four states $\sigma_{1,2} = \pm 1$ are equal (Appendix D).

III. LOGARITHMIC SUSCEPTIBILITY

We now consider the way of describing the effect of coupling to the jth oscillator on the dynamics of the ith oscillator. As seen from Eqs. (1) and (2), if the noise and the coupling of the oscillators are weak, to describe this effect, one can replace the coordinate of the jth oscillator $q_j(t)$ in the equa-

tion of motion of the ith oscillator (1) by its stable-state value $q_j(\sigma_j;t)$. In this approximation, the ith oscillator is driven by a force at frequency $\omega_p/2$ exerted by the oscillators to which it is coupled. The force changes when the jth oscillator switches between its vibrational states.

The effect of weak coupling can be understood if one considers the dynamics of an isolated parametric oscillator driven by a weak extra force $F_d\cos[(\omega_p/2)t+\phi_d]$ that mimics the force from other oscillators [24]. Such force breaks the symmetry of the vibrational states $\sigma_i=\pm1$. A major consequence of the symmetry lifting for weak force is the change of the switching rates $W_i(\sigma_i)$. To leading order in F_d this change has been predicted [45] to be described by an increment of the activation energy that is linear in F_d,

$$R_i(\sigma_i)=\bar{R}_i+\Delta R_i(\sigma_i),$$
$$\Delta R_i(\sigma_i)=\chi_i\sigma_i F_d\cos(\phi_d+\delta_i). \quad (4)$$

Here $\bar{R}_i$ is the value of $R(\sigma_i)$ in the absence of the drive. The parameters χ_i and δ_i are the magnitude and phase of the *logarithmic susceptibility*, i.e., the susceptibility of the logarithm of the switching rate. They strongly depend on the parameters of the oscillator and the parametric modulation, but are independent of F_d and ϕ_d [45].

As seen from Eqs. (3) and (4), for small noise intensity even a weak drive can significantly change the switching rates. It therefore can significantly change the stationary populations of the states. From the balance equation for the population of the ith oscillator $\dot{w}_i(\sigma_i)=-W_i(\sigma_i)w_i(\sigma_i)+W_i(-\sigma_i)w_i(-\sigma_i)$ we obtain for its stationary populations the expression

$$w_{i;\mathrm{st}}(\sigma_i)=W_i(-\sigma_i)/[W_i(\sigma_i)+W_i(-\sigma_i)].$$

Equation (4) shows that, for a parametric oscillator, a drive at half the modulation frequency plays the same role as a static field applied to an Ising spin. Consider a spin aligned along the z axis and assume that an additional field h_z is applied. The energy change is $-h_z\sigma^z$. If the spin is subject to thermal noise, its switching rate $W(\sigma^z)$ acquires an extra factor $\exp(-2h_z\sigma^z/k_BT)$. Comparing this expression to Eq. (4) and taking into account that, for the oscillator, the noise intensity D plays the role of k_BT, we see that h_z can be associated with $\chi_i\sigma_i F_d\cos(\phi_d+\delta_i)/2$. It is proportional to the drive amplitude F_d.

For a parametrically driven micromechanical oscillator, a strong population change that periodically depends on phase ϕ_d was seen in experiments [46]. However, the general effect of the linear dependence of $\log[W(\sigma_i)]$ on the drive amplitude of a periodic force in bistable systems has not been demonstrated other than in simulations [47]. This effect may be responsible for the deviation of the escape rate from the expected quadratic dependence on the drive amplitude in Josephson junctions [48].

We measure the logarithmic susceptibility of each resonator in our two-resonator system. By setting $V_{\mathrm{cpl}}=0\,\mathrm{V}$ we ensure there is no coupling between the two resonators. For each resonator, we apply a resonant drive $F_d\cos[(\omega_p/2)t+\phi_d]$ on top of the parametric modulation at ω_p. The drive phase ϕ_d is chosen to be 3.3° so that the results can be compared to the case of coupled oscillators when coupling is later re-introduced. Figure 2(a) shows the random switches

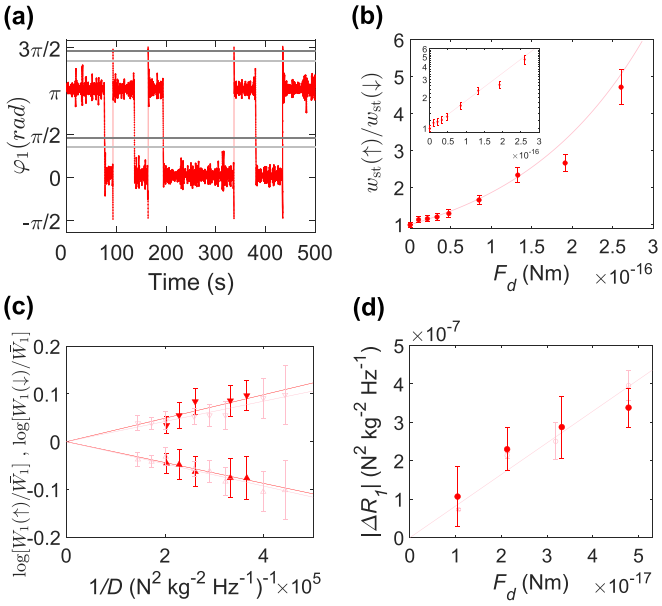

FIG. 2. Measurement of the logarithmic susceptibility of a single resonator. Coupling between the two resonators is turned off. We present results for resonator 1 and indicate the states $\sigma_1=1$ and $\sigma_1=-1$ by ↑ and ↓, respectively. (a) In the presence of noise, resonator 1 randomly switches between two coexisting vibration states with opposite phase. The two light-grey lines are thresholds for identifying phase switches. The dark-grey lines represent another choice of threshold (see Appendix C). A drive at half the modulation frequency with amplitude $F_d=1.04\times10^{-17}$ Nm breaks the symmetry and renders the residence times, and thus the stationary populations of the states ↑ and ↓ different. (b) The ratio $w_{\mathrm{st}}(\uparrow)/w_{\mathrm{st}}(\downarrow)$ increases as F_d increases. Circles are measured results for the chosen drive phase $\phi_d=3.3°$. The solid line represents theory calculated using the simulated logarithmic susceptibility. Inset: same data shown in semilog scale. (c) Logarithm of the ratio of the switching rates from states ↑ and ↓ with the resonant drive turned on, $W_1(\uparrow)$ and $W_1(\downarrow)$ (up and down triangles, respectively), to the rate with no drive $\bar{W}_1=C_1\exp(-\bar{R}_1/D)$, plotted as a function of $1/D$. The switching rates are modified by different amounts for the two states according to Eq. (4). The increments of the effective activation energies $\Delta R_1(\uparrow)$ and $\Delta R_1(\downarrow)$ are obtained from the slopes of the linear fits through the origin. (d) Increment $|\Delta R_1|$ as a function of F_d for resonator 1. The slope of the linear fit through the origin yields $\chi_1\cos(\phi_d+\delta_1)$ defined in Eq. (4). Measurements are shown in red. Numerical simulations are shown in pink.

of the phase of resonator 1 as a function of time at a constant F_d of 1.04×10^{-17} Nm. The ratio of populations $w_{\mathrm{st}}(\sigma_1=+1)/w_{\mathrm{st}}(\sigma_1=-1)\equiv w_{\mathrm{st}}(\uparrow)/w_{\mathrm{st}}(\downarrow)$ is obtained by measuring the residence time in the two states $\sigma_1=\pm1$. Figure 2(b) shows that this ratio deviates from 1 as F_d is increased.

Next, the switching rates are measured by fitting to the Poisson distribution of the residence times (Appendix C). Figure 2(c) shows the effect of $1/D$ (which mimics the inverse noise temperature) on the logarithm of the ratio of switching rates with the symmetry breaking drive turned on and off. The upper and lower branches represent decrease and increase of the activation energy respectively, corresponding to opposite signs of σ_1 in Eq. (4). We obtain the increment

$|\Delta R_1|$ from the average of the magnitude of the slopes of the two linear fits through the origin. The linear dependence of $\log[W_1(\sigma_1)/\bar{W}_1]$ on $1/D$ in Fig. 2(c) confirms that the effect of a weak symmetry-breaking drive is primarily a change $\Delta R_1(\sigma_1)$ of the activation energy of interstate switching. If D is small compared to $|\Delta R_1|$, the change of the switching rate can be substantial. As shown in Fig. 2(d), $|\Delta R_1|$ is indeed linear in F_d for a weak drive. The factor $\chi_1 \cos(\phi_d + \delta_1)$ for resonator 1 is given by the slope of the linear fit (solid-red line). Measurements are then repeated for resonator 2 to yield $\chi_2 \cos(\phi_d + \delta_2)$.

In Fig. 2(d) the measurements are compared with the results of simulations of the switching rate. There is excellent agreement between measurement and the general expressions (3) and (4). For stronger drive the stable vibrational states of the resonators change significantly and the dependence of $\log[W_i(\sigma_i)]$ on F_d becomes nonlinear (Appendix F).

IV. DYNAMICS OF COUPLED PARAMETRIC OSCILLATORS

It follows from the above results that, if we now consider coupled oscillators, the rate of switching $\sigma_i \to -\sigma_i$ of the ith oscillator depends on the states $\{\sigma_j\}$ of the oscillators coupled to it. Since the resonant force on the ith oscillator from the jth oscillator is $V_{ij} q_j(\sigma_j; t)$, from Eqs. (2)–(4), for weak coupling we have

$$W_i(\sigma_i, \{\sigma_{j\neq i}\}) = \bar{W}_i \exp\left[-\sum_{j\neq i} K_{ij}\sigma_i\sigma_j\right], \tag{5}$$

$$K_{ij} = -V_{ij}\chi_i A_j \cos(\phi_j + \delta_i)/D_i, \tag{6}$$

where $\bar{W}_i = C_i \exp(-\bar{R}_i/D_i)$ is the switching rate in the absence of coupling. The change of the activation energy $\Delta R_i(\sigma_i, \{\sigma_{j\neq i}\})$ is equal to $\sum_{j\neq i} K_{ij}\sigma_i\sigma_j D_i$.

Equation (5) has the form of the expression for the switching rates of coupled Ising spins. In the standard Ising model K_{ij} is given by the ratio of the coupling energy J_{ij} to $k_B T$ [41]. Therefore $K_{ij} = K_{ji}$. In our case, if all oscillators are identical, we also have $K_{ij} = K_{ji}$, as seen from Eq. (6). Therefore the system of coupled identical parametric oscillators maps onto the standard Ising model of coupled spins.

If the oscillators are different, $K_{ij} \neq K_{ji}$. As $V_{ij} = V_{ji}$ in Eq. (6), the difference originates from both the vibration amplitudes and logarithmic susceptibilities. For $K_{ij} \neq K_{ji}$, the system is mapped onto the *asymmetric Ising model*. As seen from the known expressions for the vibration amplitudes and phases as well as the logarithmic susceptibilities (cf. [45]), the difference between K_{ij} and K_{ji} can be already large if, for example, the oscillator eigenfrequencies are slightly different: $|\omega_i - \omega_j| \ll \omega_i$, but the ratio $|\omega_i - \omega_j|/\Gamma_i$ is not small and, importantly, the noise intensity is small.

A. The balance equation

We can now consider the distribution $w(\sigma_1, \sigma_2, ...) \equiv w(\{\sigma_i\})$ of the spins over their states, i.e., the distribution of the coupled oscillators over their vibrational states. The evolution of this distribution is described by the balance equation, which can be written in the form

$$\dot{w}(\{\sigma_i\}) = -\sum_i \sigma_i \times \sum_{\sigma_i'} \sigma_i' [W_i(\sigma_i', \{\sigma_{j\neq i}\}) w(\sigma_i', \{\sigma_{j\neq i}\})], \tag{7}$$

with the switching rates given by Eq. (5). Even if the rates $\bar{W}_i$ are different for different spins (different parametric oscillators), but the model is symmetric, $K_{ij} = K_{ji}$, Eq. (7) has the stationary solution $w_{\rm st}(\{\sigma_i\}) = \text{const} \times \exp[\frac{1}{2}\sum_{i,j} K_{ij}\sigma_i\sigma_j]$, which has the form of the thermal distribution of the conventional symmetric Ising model. This solution does not apply if $K_{ij} \neq K_{ji}$.

The time dependence of $w(\{\sigma_i\})$ is determined by the eigenvalues of the $2^N \times 2^N$ matrix $W_i(\sigma_i, \{\sigma_{j\neq i}\})$, where N is the number of spins. For a symmetric Ising model all eigenvalues of this matrix are real. To see this, we change in Eq. (7) from the distribution w to $\tilde{w}$,

$$w(\{\sigma_i\}) = \exp\left(\frac{1}{4}\sum_{i,j} K_{ij}\sigma_i\sigma_j\right)\tilde{w}(\{\sigma_i\}).$$

For $K_{ij} = K_{ji}$, the balance equation for the function $\tilde{w}$ reads

$$\frac{d}{dt}\tilde{w}(\{\sigma_i\}) = -\sum_i W_i(\sigma_i, \{\sigma_{j\neq i}\})\,\tilde{w}(\{\sigma_i\}) + \sum_i \bar{W}_i\,\tilde{w}(-\sigma_i, \{\sigma_{j\neq i}\}). \tag{8}$$

The off-diagonal elements of the matrix in the right-hand side are given by $\bar{W}_i$. They are independent of the spin state and are thus the same for $\sigma_i = 1$ and $\sigma_i = -1$. Therefore all eigenvalues of Eq. (8), and thus also of Eq. (7), are indeed real. For an asymmetric Ising model the eigenvalues of the matrix of the transition rates can be complex, see Sec. V A 1. This is another significant difference between symmetric and asymmetric Ising models.

It is seen from Eq. (7) that the trace of the distribution $w(\{\sigma_i\})$ is conserved, $\sum_{\{\sigma_i\}} \dot{w}(\{\sigma_i\}) = 0$. This shows that one of the eigenvalues of the matrix $W_i(\sigma_i, \{\sigma_{j\neq i}\})$ is zero. The corresponding eigenvector is the stationary probability distribution $w_{\rm st}(\{\sigma_i\})$, which we normalize, $\sum_{\{\sigma_i\}} w_{\rm st}(\{\sigma_i\}) = 1$. The distribution $w_{\rm st}(\{\sigma_n\})$ is generally not known for an asymmetric Ising model. Its structure is significantly different from that for a symmetric model even where the asymmetry is weak, see Appendix H.

From Eqs. (5) and (6) we see that the switching rates do not change if all spins change sign. We note that the rates of switching between the states $\sigma \to -\sigma$ ($\sigma = \pm 1$) of an isolated spin (isolated parametric oscillator) are the same by symmetry. For coupled oscillator the symmetry is restored if the signs of all σ_i are changed. A consequence of this symmetry seen from Eq. (7) is that, in the stationary regime, the distribution also does not change if all spins change signs,

$$W_i(\sigma_i, \{\sigma_{j\neq i}\}) = W_i(-\sigma_i, \{-\sigma_{j\neq i}\}),$$
$$w_{\rm st}(\{\sigma_i\}) = w_{\rm st}(\{-\sigma_i\}) \tag{9}$$

(we do not consider spontaneous symmetry breaking that may occur in an infinite system).

B. The probability current

The lack of detailed balance in the asymmetric Ising model can be shown without knowing the stationary distribution. One has to compare the ratio of the rates of flipping an ith spin back and forth directly or with a kth spin flipped back and forth on the way. For a system with detailed balance the result should be the same. We now compare these ratios. To shorten the notations, we keep in the expressions for the rates only the directly involved spins σ_i and σ_k and explicitly indicate which of them is flipped; other spins are not flipped. The detailed balance condition reads

$$\frac{W(\sigma_i,\sigma_k\to-\sigma_i,\sigma_k)}{W(-\sigma_i,\sigma_k\to\sigma_i,\sigma_k)}=\frac{W(\sigma_i,\sigma_k\to\sigma_i,-\sigma_k)}{W(-\sigma_i,\sigma_k\to-\sigma_i,-\sigma_k)}\times\frac{W(\sigma_i,-\sigma_k\to-\sigma_i,-\sigma_k)}{W(-\sigma_i,-\sigma_k\to\sigma_i,-\sigma_k)}\times\frac{W(-\sigma_i,-\sigma_k\to-\sigma_i,\sigma_k)}{W(\sigma_i,-\sigma_k\to\sigma_i,\sigma_k)}. \quad (10)$$

For an asymmetric Ising model the equality does not hold: it follows from Eq. (6) that the ratio of the right-hand side to the left-hand side is $\exp[4(K_{ik}-K_{ki})\sigma_i\sigma_k]$. The result is independent of the switching rates $\bar{W}_i, \bar{W}_k$ in the absence of coupling.

Directly related to the lack of detailed balance is the onset of a probability current in the stationary state. An elementary transition is a flip of a single spin, with the rate that depends on other spins. In the stationary state, the current associated with the rates of flipping the ith spin back and forth for a given configuration of other spins $\{\sigma_{j\neq i}\}$ is

$$\begin{aligned}&I(\sigma_i,\{\sigma_{j\neq i}\}\to-\sigma_i,\{\sigma_{j\neq i}\})\\&\quad=w_{\rm st}(\sigma_i,\{\sigma_{j\neq i}\})\,W_i(\sigma_i,\{\sigma_{j\neq i}\})\\&\qquad-w_{\rm st}(-\sigma_i,\{\sigma_{j\neq i}\})\,W_i(-\sigma_i,\{\sigma_{j\neq i}\}).\end{aligned} \quad (11)$$

For symmetric coupling, $K_{ij}=K_{ji}$, the current (11) is zero (Appendix G).

We note that the onset of current is not necessarily related to the disorder in the underlying system of oscillators. A periodic nonreciprocal systems that displays the probability current is described in Sec. VI.

V. THE STATIONARY DISTRIBUTION AND THE PROBABILITY CURRENT FOR TWO COUPLED MICROMECHANICAL RESONATORS

A. Explicit expressions

We now relate the general expressions to the system of two coupled parametric oscillators studied in the experiment. In this case the stationary probability distribution of the corresponding spins and the probability current can be found in the explicit form. Because of the symmetry with respect to changing the signs of all spins (9), it suffices to give the stationary distribution $w_{\rm st}(\sigma_1,\sigma_2)$ for $\sigma_1=\sigma_2$ and $\sigma_1=-\sigma_2$,

$$\begin{aligned}w_{\rm st}(1,1)&=\frac{1}{4}\frac{\bar{W}_1\exp(K_{12})+\bar{W}_2\exp(K_{21})}{\bar{W}_1\cosh(K_{12})+\bar{W}_2\cosh(K_{21})},\\w_{\rm st}(1,-1)&=\frac{1}{4}\frac{\bar{W}_1\exp(-K_{12})+\bar{W}_2\exp(-K_{21})}{\bar{W}_1\cosh(K_{12})+\bar{W}_2\cosh(K_{21})}.\end{aligned} \quad (12)$$

For a symmetric system, $K_{12}=K_{21}=K$, we have $w_{\rm st}(1,1)/w_{\rm st}(1,-1)=\exp(-2K)$ independent of the values of $\bar{W}_{1,2}$, whereas for an asymmetric system the populations depend not only on the coupling parameters K_{ij}, but also on the interrelation between the switching rates of the oscillators in the absence of coupling $\bar{W}_1$ and $\bar{W}_2$.

From Eqs. (11) and (12), the stationary probability current in the two-spin system is

$$I(1,1\to1,-1)=\frac{\bar{W}_1\bar{W}_2}{2}\frac{\sinh(K_{12}-K_{21})}{\bar{W}_1\cosh(K_{12})+\bar{W}_2\cosh(K_{21})} \quad (13)$$

[here we use ±1 to indicate the values of the spins σ_1 and σ_2; $I(1,1\to1,-1)\equiv I(\sigma_1=1,\sigma_2=1\to\sigma_1=1,\sigma_2=-1)$]. As expected, the current is zero in a symmetric system, $K_{12}=K_{21}$. Note the Kirchhoff's rule,

$$\begin{aligned}I(1,1\to1,-1)&=I(1,-1\to-1,-1)\\&=I(-1,-1\to-1,1)\\&=I(-1,1\to1,1).\end{aligned} \quad (14)$$

This equation shows that the current flows along the loop of the states of two spins.

Approaching the equilibrium

For a system of two coupled spins we find from Eq. (7) that the nonzero eigenvalues are

$$\begin{aligned}\lambda_2&=-2(\bar{W}_1\cosh K_{12}+\bar{W}_2\cosh K_{21}),\\\lambda_{3,4}&=\tfrac{1}{2}\lambda_2\pm\left[\tfrac{1}{4}\lambda_2^2-4\bar{W}_1\bar{W}_2\cosh(K_{12}-K_{21})\right]^{1/2}.\end{aligned} \quad (15)$$

We see that $\mathrm{Re}\,\lambda_{2,3,4}<0$, which indicates that the system approaches a stationary state with increasing time. However, the roots $\lambda_{3,4}$ can be complex; for example, for $\bar{W}_1=\bar{W}_2=\bar{W}$ and $K_{12}=-K_{21}=K$ we have $\lambda_{3,4}=-2\bar{W}(\cosh J\pm i\sinh J)$. This case corresponds to the parameters K_{12} and K_{21} having opposite signs. For coupled parametric oscillators K_{ij} and K_{ji} are proportional to the same coupling constant, and therefore they have the same signs, so that the eigenvalues (15) are real.

B. The experiment

A central part of this paper is the demonstration of the asymmetry in the coupling coefficients and the existence of a probability current using our system of two coupled parametric oscillators ($i=1,2$). Weak coupling between the two resonators is introduced by applying $V_{\rm cpl}=0.3\,\mathrm{V}$. We adjust the dc voltages on the right electrodes of the resonators to tune the resonant frequencies to be close but nonidentical, with $\omega_1-\omega_2=0.4\,\mathrm{Hz}$. The two resonators are subjected to parametric modulation of the same amplitude and the same frequency ω_p. As shown in Fig. 3(a), when ω_p is swept up, resonator 2 undergoes a subcritical bifurcation first, followed by resonator 1. The electrostatic coupling between the two plates favors the configuration where the phases of the resonators are opposite to each other. In the absence of injected noise, resonator 1 adopts a vibration phase opposite to resonator 2 as ω_p is increased. Correlations in the phase were previously observed in two nanomechanical parametric resonators [16]

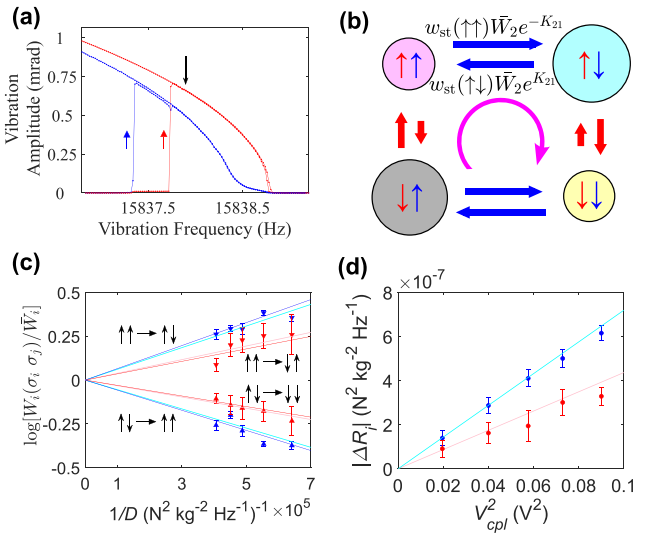

FIG. 3. Implementation of an asymmetric Ising model with two nonidentical coupled parametric oscillators. (a) Vibration amplitudes of resonators 1 (red) and 2 (blue), with $\Delta\omega/2\pi = -0.4$ Hz and $V_{\rm cpl} = 0.3$ V, under identical parametric modulation with no noise added. The black arrow marks $\omega_p/2$ for measuring noise-induced switching for the rest of the figure. Rotation angle of 1 mrad corresponds to displacement of 100 nm at the edge of the plate. (b) Switchings between the four states of the two-resonator system in the presence of noise. The areas of the circles are proportional to the measured stationary populations $w_{\rm st}(\sigma_1,\sigma_2)$ (the first arrow from the left refers to σ_1 and the second arrow refers to σ_2). The lengths of the straight arrows between the circles are proportional to the products of the measured switching rates $W_i(\sigma_1,\sigma_2)$ and the corresponding populations $w_{\rm st}(\sigma_1,\sigma_2)$. The purple arrow represents the net probability current. (c) Logarithm of the measured changes of the switching rates due to coupling as a function of $1/D$. The values of $\Delta R_i(\sigma_i,\sigma_j) \equiv -D\log[W_i(\sigma_i,\sigma_j)/\bar{W}_i]$ are determined by the slopes of the linear fits. The difference between $|\Delta R_1(\sigma_1,\sigma_2)|$ and $|\Delta R_2(\sigma_2,\sigma_1)|$ for the same pairs (σ_1,σ_2) is identified from the different magnitudes of the slopes. This difference determines the asymmetry of the Ising model. (d) Dependence of $|\Delta R_i|$ (red) and $|\Delta R_2|$ (blue) on $V_{\rm cpl}^2$ that is proportional to the coupling constant. The values of $|\Delta R_i|$ are the average values of $|\Delta R_i(\sigma_i,\sigma_j)|$ for $\sigma_i = \sigma_j$ and $\sigma_i = -\sigma_j$. The pink and light blue lines are obtained from theory based on the independently simulated logarithmic susceptibilities of individual uncoupled resonators.

undergoing supercritical bifurcations. Unlike Ref. [16] where the amplitude increases from zero in a continuous fashion, for the frequency up-sweep in our measurement the amplitudes jump sharply from zero in a subcritical bifurcation.

Next, we fix ω_p at $2\omega_2$ and increase the noise intensity while maintaining the same effective temperatures in the two resonators, $D_1 = D_2 = D$. The noise induces switching of each of the two resonators at random times. We measure the time intervals during which each of the four vibrational states of the two-resonator system is occupied and obtain the stationary probability distributions $w_{\rm st}(\sigma_1,\sigma_2)$. For brevity we indicate in Fig. 3 the states of each resonator $\sigma = 1$ and $\sigma = -1$ by $\uparrow$ and $\downarrow$, respectively, as we also did in Fig. 2. Therefore the four states are $\uparrow\uparrow$, $\uparrow\downarrow$, $\downarrow\uparrow$, and $\downarrow\downarrow$.

We find that, after a transient time, the state populations become time-independent. The areas of the circles in Fig. 3(b) are proportional to the measured stationary probability distribution. We find that $w_{\rm st}(\uparrow\downarrow)$ and $w_{\rm st}(\downarrow\uparrow)$ are equal, as expected by symmetry arguments, and that they exceed $w_{\rm st}(\uparrow\uparrow)$ and $w_{\rm st}(\downarrow\downarrow)$. This result is consistent with notion that the electrostatic coupling favors opposite vibration phases in the two resonators, so that $K_{12}, K_{21} < 0$.

To compare the result with the theory, it is necessary to independently determine the rates $\bar{W}_{1,2}$ and the coupling parameters K_{12} and K_{21}. For two coupled resonators, there are a total of eight transitions, as illustrated in Fig. 3(b). In the experiment, each of the eight switching rates is individually measured, by fitting to the Poisson distribution of the residence times (Appendix C). Measurements are performed both before and after the coupling is turned on to give $\bar{W}_i$ and $W_i(\sigma_i,\sigma_j)$ respectively [for two resonators, we use the notation $W_i(\sigma_i,\sigma_j)$ rather than $W_i(\sigma_i,\{\sigma_j\})$]. The ratio $W_i(\sigma_i,\sigma_j)/\bar{W}_i$ represents the modification of the switching rate of resonator i due to coupling.

Figure 3(c) plots the logarithm of the ratio $W_i(\sigma_i,\sigma_j)/\bar{W}_i$ for the two resonators as a function of $1/D$, where red and blue results correspond to switching of resonator 1 and 2 respectively. For the upper branches where the phases are identical, the switching rates are increased due to coupling, and vice versa for the lower branches. The lines are linear fits through the origin from which the change of the activation barriers ΔR_i can be obtained by taking the negative values of the slopes.

We observe that, in agreement with Eq. (9),

$$W_i(\sigma_i,\sigma_j) = W_i(-\sigma_i,-\sigma_j) \tag{16}$$

within the measurement uncertainty. Therefore in Fig. 3(c) we show the logarithm of the ratio of the average values of $W_i(\sigma_i,\sigma_j)$ and $W_i(-\sigma_i,-\sigma_j)$ to $\bar{W}_i$.

There is a clear difference between the measured values of $|\Delta R_1|$ and $|\Delta R_2|$ for the same sets (σ_1,σ_2). For resonator 1, the slopes measured in Fig. 3(c) are 3.6×10^{-7} N^{2}kg^{-2}Hz^{-1} and -3.0×10^{-7} N^{2}kg^{-2}Hz^{-1} for $\sigma_1 = \sigma_2$ and $\sigma_1 = -\sigma_2$, respectively, whereas those for resonator 2 are 6.6×10^{-7} N^{2}kg^{-2}Hz^{-1} and -5.8×10^{-7} N^{2}kg^{-2}Hz^{-1} for $\sigma_1 = \sigma_2$ and $\sigma_1 = -\sigma_2$, respectively. Averaging the magnitude of the slopes $\Delta R_i(\sigma_i,\sigma_j)$ for $\sigma_i = \sigma_j$ and $\sigma_i = -\sigma_j$ yields $|\Delta R_1|$ exceeding $|\Delta R_2|$ by a factor of 1.7. The difference between $|\Delta R_1|$ and $|\Delta R_2|$ demonstrates that our system of two parametric resonators with different resonant frequencies maps onto the asymmetric Ising model.

Figure 3(d) shows that $|\Delta R_1|$ and $|\Delta R_2|$ are proportional to the square of potential difference $V_{\rm cpl}$ between the two vibrating plates, with different proportionality constants for the two resonators. The measured values of $|\Delta R_i|$ are compared in Fig. 3(d) with Eq. (6) evaluated with the numerically simulated values of the logarithmic susceptibility and the vibration amplitudes and phases A_j, ϕ_j independently calculated for each resonator in the absence of coupling. There is good agreement between the entirely independent measurements with the coupling (circles) and the simulations with no coupling [the lines based on Eq. (6)]. In turn, the simulations with no coupling are in excellent agreement with the measurement of the logarithmic susceptibility with no coupling, as seen

from Fig. 2. The linear dependence of $\log[W_i(\sigma_i, \sigma_j)/\bar{W}_i]$ on $1/D$ in Fig. 3(c) confirms the proposed mechanism of the strong effect of even weak coupling, provided the noise is also weak.

As discussed earlier, a difference between $|\Delta R_1|$ and $|\Delta R_2|$, and hence K_{12} and K_{21}, implies that detailed balance is broken, giving rise to a net probability current. In the experiment, the probability currents are obtained by taking the product of the measured stationary probability distribution and the measured switching rate out of the specific state. They are represented by block arrows in Fig. 3(b). The lengths of the arrows are chosen to be proportional to the product of the measured stationary probability distribution and the measured switching rate. Our measurement demonstrates the lack of detailed balance, as evident from the difference in length of each pair of arrows. The magnitude of the net probability current for the four branches are identical within the measurement uncertainty (Appendix E). As denoted by the purple arrow in Fig. 3(b), the net probability current flows in the clockwise direction for $\omega_2 - \omega_1 = -0.4$ Hz.

1. The correlation function

The explicit solution of the balance equation allows one to calculate the correlation functions of the spins. For a two-spin system the relevant nontrivial correlator is $\langle\sigma_1\sigma_2\rangle$. From the explicit form of the stationary distribution given by Eq. (12) we find

$$\langle\sigma_1\sigma_2\rangle = 2[w_{\rm st}(1,1) - w_{\rm st}(1,-1)] = \frac{\bar{W}_1 \sinh K_{12} + \bar{W}_2 \sinh K_{21}}{\bar{W}_1 \cosh K_{12} + \bar{W}_2 \cosh K_{21}}. \quad (17)$$

For small $|K_{12}|, |K_{21}|$ the correlator (17) is linear in K_{12}, K_{21}, whereas if K_{12}, K_{21} are large and have the same sign $\langle\sigma_1\sigma_2\rangle \approx \mathrm{sgn} K_{12}$.

We compared Eq. (17) with the measured $\langle\sigma_1\sigma_2\rangle$ as a function of the coupling, with the independently measured parameters. The good agreement provides an extra proof of the consistence of the evaluation of the stationary distribution and of the picture of switching oscillators as a whole.

2. Effect of the frequency detuning of the oscillators

In our system of two coupled resonators with near identical damping, the sign and magnitude of the probability current are largely determined by the frequency mismatch $\Delta\omega = \omega_2 - \omega_1$ if the coupling and the noise intensity are fixed. When $\Delta\omega$ is changed to 0.4 Hz by adjusting the electrode potentials, we find that the sign of the net probability current is reversed. Figure 4(a) plots the net probability current averaged over the four branches as a function of $\Delta\omega$. The line represents the probability current predicted by Eq. (13) with K_{12} and K_{21} given by the simulated value of the logarithmic susceptibility of a single resonator using Eq. (6).

The difference between K_{12} and K_{21}, and hence the probability current, can be tuned to zero by choosing $\Delta\omega$. In our system, choosing $\Delta\omega$ equal to zero makes the probability current vanish within measurement uncertainty. Detail balance is restored. The two resonators therefore map to the symmetric Ising model (Appendix G). The stationary

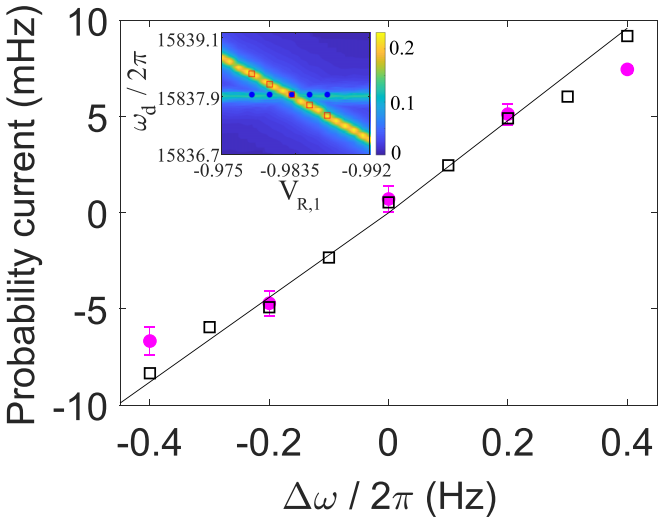

FIG. 4. Dependence of probability current on the frequency mismatch $\Delta\omega$ between the two resonators at $V_{\rm cpl} = 0.3$ V. Purple circles are measurement. Calculations for two resonators based on the simulated logarithmic susceptibility of individual units are plotted in black. The straight line is a linear fit through the origin. (Inset) For the considered weak coupling the frequency anticrossing as a function of $\omega_2 - \omega_1$ is undetectable. The color represents the amplitudes of forced vibrations of the two modes in mrad; x axis is the bias $V_{R,1}$ (V) that controls ω_1, whereas y axis is the frequency of resonant drive (Hz) applied to both resonators. Red squares and blue circles mark the values of ω_1 and ω_2 used in the main figure.

distribution $w_{\rm st}$ found in the experiment in this case coincides with the standard expression $w_{\rm st}(\{\sigma_i\}) \propto \exp(\sum K_{ij}\sigma_i\sigma_j/2)$. We further show in Appendix G that, while $w_{\rm st}(\uparrow\downarrow) = w_{\rm st}(\downarrow\uparrow)$ exceed $w_{\rm st}(\uparrow\uparrow) = w_{\rm st}(\downarrow\downarrow)$ due to the coupling, the switching rates given by Eq. (11) lead to vanishing of the net probability current.

VI. PERIODIC ASYMMETRIC GLAUBER CHAIN

Along with the random disorder generally inherent to a system of coupled parametric oscillators, an asymmetric Ising model can be implemented with a more intricate system in which the disorder is constructed. A simple and important example is where groups of two different oscillators are repeated periodically. If the oscillators form a chain with nearest-neighbor coupling, they can be mapped on a spin chain in which every other spin is the same, but the coupling of the spins on the even sites to those on the odd sites differs from the coupling of the spins on the odd sites to those on the even sites,

$$K_{2i\,2i\pm1} = K_{\rm e},\ K_{2i+1\,2i+1\pm1} = K_{\rm o} \quad (K_{\rm o} \neq K_{\rm e}).$$

We set the switching rates in the absence of the coupling to be periodic, too,

$$\bar{W}_{2i} \equiv \bar{W}_{\rm e}, \quad \bar{W}_{2i+1} = \bar{W}_{\rm o}, \quad \forall i.$$

In the spirit of the Glauber work on the Ising model [41] we will concentrate on the dynamics for weak coupling,

$|K_{ij}| \ll 1$, so that

$$W_i(\sigma_i, \{\sigma_{j\neq i}\}) \approx \bar{W}_i(1 - K_{i\,i+1}\sigma_i\sigma_{i+1} - K_{i\,i-1}\sigma_i\sigma_{i-1}). \quad (18)$$

The chain has two spins per unit cell. If it is periodic and the number of cells is N [that is, in Eq. (18) $i = 1, 2, ..., 2N$ and $\sigma_{i+2N} = \sigma_i$], we can switch to the Fourier representation of the average spins

$$\sigma_{\rm e}(k) = \sum_{n=1}^{N} e^{2ink}\langle\sigma_{2n}\rangle, \quad \sigma_{\rm o}(k) = \sum_{n=1}^{N} e^{ik(2n-1)}\langle\sigma_{2n-1}\rangle.$$

The equations for the Fourier components for periodic boundary conditions read

$$\begin{aligned} \frac{1}{\bar{W}_{\rm e}}\frac{d}{dt}\sigma_{\rm e}(k) &= -\sigma_{\rm e}(k) + 2K_{\rm e}\sigma_{\rm o}(k)\cos k, \\ \frac{1}{\bar{W}_{\rm o}}\frac{d}{dt}\sigma_{\rm o}(k) &= -\sigma_{\rm o}(k) + 2K_{\rm o}\sigma_{\rm e}(k)\cos k. \end{aligned} \quad (19)$$

Equations (19) describe diffusion waves that propagate in the chain. Such waves decay in time, for a given k, that is, if we consider a wave $\propto \exp[ikn - i\omega(k)t]$, the "eigenfrequency" $\omega(k)$ has an imaginary component. Because there are two spins per unit cell, there are two branches of the diffusion waves. Their eigenfrequencies are

$$\begin{aligned} \omega_{1,2}(k) = &-\tfrac{1}{2}i(\bar{W}_{\rm e} + \bar{W}_{\rm o}) \pm \tfrac{1}{2}i[(\bar{W}_{\rm e} - \bar{W}_{\rm o})^2 \\ &+ 16\bar{W}_{\rm e}\bar{W}_{\rm o}K_{\rm e}K_{\rm o}\cos^2 k]^{1/2}. \end{aligned} \quad (20)$$

Since the parameters $|K_{\rm e,o}|$ are small, $\mathrm{Im}\,\omega_{1,2}(k) < 0$, i.e., diffusion waves decay in time in our nonequilibrium system, as expected. A qualitative feature of the system is that this decay can be accompanied by temporal oscillations. This occurs if $\mathrm{Re}\,\omega(k) \neq 0$. In turn, this requires that $K_{\rm e}K_{\rm o} < 0$, i.e., $K_{2i\,2i\pm1}$ and $K_{2i+1\,2i+1\pm1}$ have opposite signs. Also, for small $|K_{\rm e,o}|$ this requires that the switching rates in the absence of coupling be close, $|\bar{W}_{\rm e} - \bar{W}_{\rm o}| \ll \bar{W}_{\rm e,o}$. As noted earlier, for parametric oscillators the coupling parameters K_{ij} and K_{ji} have the same sign, and therefore the frequencies (20) are imaginary.

To the lowest order in the coupling $K_{\rm e,o}$ the stationary distribution of the periodic chain is

$$w_{\rm st} \approx Z^{-1}\exp\left[\frac{\bar{W}_{\rm e}K_{\rm e} + \bar{W}_{\rm o}K_{\rm o}}{\bar{W}_{\rm e} + \bar{W}_{\rm o}}\sum_i \sigma_{2i}(\sigma_{2i+1} + \sigma_{2i-1})\right]. \quad (21)$$

To the zeroth order in the coupling the partition function is $Z \to Z_0 = 2^{2N}$. We emphasize that the solution (21) only works to the lowest order in $K_{\rm e}$, $K_{\rm o}$. Beyond this approximation the distribution $w_{\rm st}$ cannot be written in the simple Ising form of the exponential of the sum $\sum_i \sigma_{2i}(\sigma_{2i+1} + \sigma_{2i-1})$.

Even though the chain is periodic, there is still a nonzero probability current. For example, the current for the flip of an even-site spin while the surrounding spins have the same orientation as this spin is

$$\begin{aligned} &I(\sigma_{2i} = \sigma_{2i\pm1} = 1 \to \sigma_{2i} = -1, \sigma_{2i\pm1} = 1) \\ &\quad = \frac{\bar{W}_{\rm e}\bar{W}_{\rm o}}{2(\bar{W}_{\rm e} + \bar{W}_{\rm o})}(K_{\rm o} - K_{\rm e}). \end{aligned} \quad (22)$$

Here we have taken into account that we have to sum over all spin configurations except for the spins on the sites $2i-1, 2i, 2i+1$. Equation (22) shows that, if spins on the "odd" sites are "stronger", $K_{\rm o} > K_{\rm e}$, and are aligned, $\sigma_{2i+1} = \sigma_{2i-1}$, the probability current flows from the configuration where even-site spins are parallel to odd-site ones to the configuration where they are antiparallel.

The even-odd configuration can be easily extended to a square lattice. This opens a question of the onset of "magnetization" in a large periodic system depending on the asymmetry. Such magnetization may correspond to the parametric oscillators vibrating in phase or, in turn, in counterphase.

VII. CONCLUSIONS

The results of the paper show that even weak coupling of parametric oscillators, where the coupling energy is small compared to the energy of the parametrically excited vibrations, leads to unexpectedly rich features of the system. These features come from interplay of the coupling, small fluctuations, and small differences between the oscillator eigenfrequencies. For an isolated oscillator, fluctuations lead to occasional transitions between degenerate vibrational states with the same amplitudes and opposite phases. Coupling lifts the degeneracy, as vibrations of one oscillator bias the other oscillator to vibrate in phase or in counterphase, depending on the coupling sign. Fluctuations accentuate this bias, by allowing the oscillators to switch between the states and thus to adjust to each other. The effect of coupling on the switching rates underlies the mapping of the system on a system of coupled Ising spins, with the two projections of an individual spin corresponding to the two vibrational states of an individual oscillator. If the oscillators are not identical, they affect each other differently, so that the system maps onto the asymmetric Ising model, enabling exploring this model in a fully controlled experiment.

We found the stationary probability current in an asymmetric Ising system and measured it in a system of two coupled parametric oscillators. The current originates from the difference of the parameters of the underlying individual oscillators, or in other words, from the disorder in the system. Emergence of the current is associated with the breaking of the detailed balance. Even a small difference of the oscillator parameters can generate a substantial current provided that fluctuations are also small.

Our measurements are done in the regime where the coupling-induced change of the oscillator frequencies is much smaller than the frequencies themselves, and the noise-induced spread of the vibration amplitudes is much smaller than the amplitudes themselves. Yet the ratio of the properly scaled coupling and noise intensity can be arbitrary. We note that, for a parametrically excited oscillator, noise necessarily comes along with relaxation, so that it is present even in the quantum regime.

The experiment shows that the effect of weak coupling of parametric oscillators can be quantitatively described in terms of an entirely independent effect of an additional drive at half the modulation frequency applied to an individual oscillator. It is demonstrated that, in a broad range of the drive amplitudes, the drive leads to a change of the *logarithm* of the rate of switching between the vibrational states of the

oscillator, which is linear in the drive amplitude. To the best of our knowledge, this is the first direct measurement of the logarithmic susceptibility in a physical system. The result is found to be in excellent agreement with simulations.

We note that the effect of the drive at half the modulation frequency on a parametric oscillator is similar to the effect of a static z field on an Ising spin. Therefore a system of coupled oscillators provides a versatile platform to study the dynamics of symmetric or asymmetric Ising systems in the presence of a static field, which can be fully controlled on each spin.

The stationary state of an asymmetric Ising model is not known, generally. While the system of coupled parametric oscillators maps on the model in the presence of disorder in the oscillator parameters, a more sophisticated system can be constructed by "organizing" disorder, so that groups of two or more types of different oscillators are repeated periodically. Among other problems, such system allows addressing the problem of phase transitions in the presence of the probability current.

Our results demonstrate that a system of slightly different parametric oscillators provides a long-sought inorganic implementation of an asymmetric Ising model. The parameters of the model are determined by the oscillator parameters, including the eigenfrequencies and the coupling, as well as the amplitude and frequency of the parametric modulation. These parameters can be controlled in a broad range. For oscillators based on micro- and nanomechanical resonators, this opens a way of creating asymmetric Ising networks with variable coupling strength and variable connectivity, which is the problem of interest for diverse disciplines, from statistical physics to biology to artificial intelligence. Besides these applications, such networks provide a conceptually simple setting for studying features of many-body dynamics away from thermal equilibrium. One of the major generic features is the lack of detailed balance, which leads to the onset of a probability current in the stationary state.

ACKNOWLEDGMENTS

This work was supported by the Research Grants Council of Hong Kong SAR (Project No. 16304620) and partially supported by Project No. HKUST C6008-20E. M.I.D. was supported in part by the National Science Foundation through Grant No. DMR-2003815, the Moore Foundation through Grant No. 12214, and Google Faculty Research Award.

APPENDIX A: COUPLED PARTICLES WITH BISTABLE POTENTIALS

Here we show that, even in the presence of disorder, but in thermal equilibrium, coupling between particles in bistable potentials does not lead to mapping on the asymmetric Ising model. We consider particles with coordinates q_n in double-well potentials $U_n(q_n)$, where n enumerates the particles. We count the coordinate q_n off from the barrier top of $U_n(q_n)$. For an isolated particle, the potential $U_n(q_n)$ is symmetric and has minima at $Q_n\sigma_n$, where $\sigma_n = \pm 1$ and Q_n is the value of $|q_n|$ at the minimum,

$$U_n(q_n) = U_n(-q_n),$$
$$dU_n/dq_n = 0 \quad \text{for} \quad q_n = 0, \pm Q_n. \tag{A1}$$

The minima at $\pm Q_n$ are the stable states of the particles. Particles switch between the minima due to thermal fluctuations. For isolated particles the rates $W_n(\sigma_n)$ of interstate switching $\sigma_n \to -\sigma_n$ are the same for the both states $\sigma_n = \pm 1$, with

$$W_n(\sigma_n) = W_n(-\sigma_n) = \bar{W}_n,$$
$$\bar{W}_n = C_n \exp(-\Delta U_n/k_BT). \tag{A2}$$

Here $\Delta U_n = U_n(0) - U_n(Q_n)$ is the barrier height between the wells of $U_n(q_n)$; for a Brownian particle, the prefactor C_n has been first studied by Kramers [43].

Weak potential coupling between the particles is described by the term in the potential energy of the system, which has the form

$$U_{\rm cpl} = \frac{1}{2}{\sum_{n,m}}' V_{nm}q_nq_m \tag{A3}$$

where V_{nm} are the coupling parameters. A more general form of $U_{\rm cpl}$ does not change the results as long as we consider the case where the global symmetry $\{q_n\} \to \{-q_n\}, \forall n$, is preserved; this case is of utmost interest in terms of revealing the effect of the coupling on the system dynamics.

For low temperatures, the particles reside mostly close to the potential minima $\pm Q_n$ and only rarely switch between the minima, the rates $W_n(\sigma_n)$ are small compared to the relaxation rates. When the mth particle is close to its minimum $Q_m\sigma_m$, the potential of the nth particle is incremented by $-V_{nm}q_nQ_m\sigma_m$. Respectively, the depth of the σ_nth potential well is incremented by $V_{nm}Q_nQ_m\sigma_n\sigma_m$. As a result the rate of switching from this well becomes

$$W_n(\sigma_n, \{\sigma_{m\neq n}\}) = \bar{W}_n \exp\left(-\sigma_n \sum_{m\neq n} K_{nm}^{\rm pot}\sigma_m\right),$$
$$K_{nm}^{\rm pot} = -V_{nm}Q_nQ_m/k_BT. \tag{A4}$$

It is seen from this equation that $K_{nm}^{\rm pot} = K_{mn}^{\rm pot}$. The system of weakly coupled particles in symmetric double-well potentials maps on a symmetric Ising model, for low temperatures. It is not required that the potentials be identical. We note that the parameters $K_{nm}^{\rm pot}$ are not small for weak coupling provided the temperature is low.

The difference from bistable parametric oscillators originates from the fact that, in the case of the oscillators, the changes of the switching rates are determined not by changes of the depths of the effective potentials in the rotating frame, but by the logarithmic susceptibilities.

APPENDIX B: EXCITATION AND DETECTION SCHEMES

The top plate of each resonator i ($i = 1, 2$) is subjected to electrostatic torques exerted by the left and right electrodes. If the potential difference between the top plates $V_{\rm cpl} = V_2^{\rm top} - V_1^{\rm top}$ is nonzero, there is also an electrostatic attraction between the two top plates. Each top plate is connected to the input of an amplifier that is a virtual ground for ac voltages.

For resonator i, the total electrostatic torque from the two electrodes is given by the sum $\tau_i = \frac{1}{2}\sum_{\alpha=L,R}(dC_{\alpha,i}/d\theta_i)(V_i^{\rm top} - V_{\alpha,i})^2$, where the subscript α denotes the left (L) or the right (R) electrode, $C_{L,i}$ ($C_{R,i}$) is the capacitance between the top plate and the left (right) electrode. $V_{L,i}$ and $V_{R,i}$ are the voltages on the left and right electrodes, respectively. Expanding the torque about the initial angle $\theta_{0,i}$ gives

$$\tau_i = \frac{1}{2}\sum_{\alpha}\left[C'_{\alpha,i} + C''_{\alpha,i}\theta_i + \frac{1}{2}C'''_{\alpha,i}\theta_i^2 + \frac{1}{6}C^{IV}_{\alpha,i}\theta_i^3\right] \times \left(V_i^{\rm top} - V_{\alpha,i}\right)^2, \tag{B1}$$

where θ_i is the rotation angle of resonator i measured from $\theta_{i,0}$. C'_i, C''_i, C'''_i, and C^{IV}_i denote the derivatives of C_i with respect to θ_i, evaluated at $\theta_{0,i}$. Higher order terms are neglected.

$V_{R,i}$ contains only a dc component that is used to adjust ω_i via the electrostatic spring softening effect. $V_{L,i}$ consists of small ac voltages on top of a dc component $V^{\rm dc}_{L,i}$. It is used to control the parametric modulation, the symmetry-breaking torque and the noise torque. Considering only the dc component and the term responsible for the parametric excitation

$$V_{L,i} = V^{\rm dc}_{L,i} + V_{p,i}\cos(\omega_p t), \tag{B2}$$

where $V_{p,i} << |V_i^{\rm top} - V^{\rm dc}_{L,i}|$. To induce transitions between the two coexisting vibration states, a noise voltage $V_{n,i}(t)$ is added to $V_{L,i}$. When the logarithmic susceptibility is measured, an additional ac component $V_d\cos(\frac{\omega_p}{2}t)$ is added. Throughout the experiments we use the modulation frequency $\omega_p = 2\omega_2$ when measuring noise-induced switching in two coupled resonators.

As seen from Eqs. (B1) and (B2), the time-independent component of τ_i modifies the system parameters. The term independent of θ_i shifts the equilibrium position of $\theta_{i,0}$. The term $\frac{1}{2}\sum_\alpha C''_{\alpha,i}\theta_i\Delta V^2_{\alpha,i}$, which is linear in θ_i, leads to electrostatic spring softening due to the static potential differences, producing a shift in the resonant frequency. Here $\Delta V_{L,i} = V_i^{\rm top} - V^{\rm dc}_{L,i}$ and $\Delta V_{R,i} = V_i^{\rm top} - V_{R,i}$. The nonlinear restoring torques of $\frac{1}{4}\sum_\alpha C'''_i\theta_i^2\Delta V^2_{\alpha,i}$ and $\frac{1}{6}\sum_\alpha C^{IV}_i\theta_i^3\Delta V^2_{\alpha,i}$ modify the Duffing nonlinearity.

The time-dependent components of τ_i are responsible for the parametric modulation term and noise term in Eq. (1), with $F_p = C''_{L,i}\theta_i\Delta V_{L,i}V_{p,i}$ and $\xi_i(t) = \frac{1}{M_i}C'_i\Delta V_{L,i}V_{n,i}(t)$. For the symmetry breaking drive, $F_d = C'_i\Delta V_{L,i}V_d$.

Vibrations in each resonator are detected by measuring the change of capacitance between the top plate and the two underlying electrodes. The dc voltages described above lead to build up of charges on the top plates. As each of the top plates rotates, the capacitances with the two underlying electrodes change. Charges flowing out of the two top plates are detected independently by two separate amplifiers. The outputs of each amplifier is fed into a lock-in amplifier referenced at $\omega_p/2$.

Throughout the experiment, the dc voltages $V_2^{\rm top}$ and $V^{\rm dc}_{L,2}$ for resonator 2 are fixed at 0 V and −1.00 V respectively, so that $\Delta V_{L,2}$ is maintained constant at 1.00 V. For resonator 1, $V_{{\rm top},1}$ is changed to control the coupling with resonator 2 as explained in more details below. $V^{\rm dc}_{L,1}$ is then adjusted to maintain $\Delta V_{L,1}$ constant at −1.28 V. F_p is set to be identical for the two resonators, by choosing $V_{p,1}\Delta V_{L,1} = V_{p,2}\Delta V_{L,2}$.

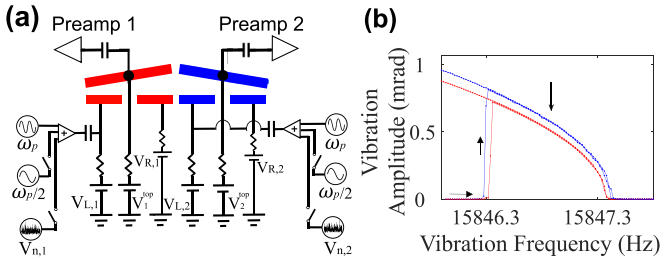

FIG. 5. (a) Schematic of the actuation scheme and measurement circuitry. Voltages applied to the left electrodes generate the parametric modulation at ω_p, the drive at $\omega_p/2$ and the noise. Voltages $V^{\rm dc}_{R,i}$ applied to the fixed electrodes allow fine tuning of the resonant frequencies. The dc voltage differences between each top plate and the underlying electrodes leads to an ac current flowing out of the top plate as it rotates. Capacitive coupling between the two plates is controlled by the voltage difference $V_1^{\rm top} - V_2^{\rm top}$. (b) Vibration amplitude of resonators 1 (red) and 2 (blue) subjected to identical parametric modulation as functions of $\omega_p/2$. There is no coupling between the resonators and the eigenfrequencies are tuned to be almost equal.

The voltages $V_{R,1}$ and $V_{R,2}$ applied to the right electrodes are used to control ω_1 and ω_2 respectively, as mentioned earlier. Unlike $V_{L,i}$, $V_{R,i}$ contains no ac components. Initially, $\Delta V_{R,1}$ and $\Delta V_{R,2}$ are chosen to be −0.5 V and 0.5 V respectively to bring ω_1 and ω_2 close to each other. Subsequently, small changes to $\Delta V_{R,1}$ and $\Delta V_{R,2}$ allow the fine tuning of $\Delta\omega$ to the desired value via the electrostatic spring softening effect discussed above. Furthermore, $V_{R,1}$ and $V_{R,2}$ are adjusted regularly to compensate for long term drifts in the resonant frequencies. The adjustment is performed by first setting $V_{\rm cpl}$ to 0 V. Subsequently, the vibration amplitude in response to the parametric modulation is measured at a specific ω_p. The changes in amplitude from the value recorded at the beginning of the experiment are used to infer the shifts in the eigenfrequencies. Small changes to $V_{R,1}$ and $V_{R,2}$ are sufficient to bring the vibration amplitudes, and hence the eigenfrequencies, back to the original values for the experiment to continue.

The two plates have identical width of 200 μm and thickness of 2 μm. Coupling between them is generated when $V_{\rm cpl} = V_1^{\rm top} - V_2^{\rm top}$ is applied to the interdigitated comb shaped electrodes with separation ranging from 3 μm to 5 μm at different locations. Even though the equilibrium positions of $\theta_{1,2}$, as counted from the horizontal axis in Fig. 5(a), are nonzero, the static rotations are small. When there are no vibrations, the sidewalls on the two plates remain largely parallel and aligned with each other. The electrostatic potential energy between the two top plates is given by $\frac{1}{2}C_{12}(\theta_1,\theta_2)V^2_{\rm cpl}$, where C_{12} is the capacitance between the two plates. If we disregard the small misalignment of the plates, C_{12} contains a term $\lambda(\theta_1-\theta_2)^2$, where λ is a proportionality constant. This term determines the coupling energy in Eq. (1). Specifically, $V_{12} = V_{21} = \lambda V^2_{\rm cpl}$. As shown in the inset in Fig. 4, level anticrossing does not occur for the small $V_{\rm cpl}$ used in this paper. The term $\propto\lambda(\theta_1^2+\theta_2^2)$ in the coupling energy leads to changes of ω_1 and ω_2, by $\delta\omega_1$ and $\delta\omega_2$ respectively, with $\delta\omega_1 \sim \delta\omega_2$. These changes are measured at the beginning of the experiment from the shifts in the peaks of the linear resonant response from

their value at $V_{\rm cpl} = 0$ V. As described earlier, in the procedure to compensate for the long term drifts in $\omega_{1,2}$, $V_{\rm cpl}$ is set to 0 V. After the compensation is completed, $V_{\rm cpl}$ needs to be changed back to the target value. The previously recorded values of $\delta\omega_{1,2}$ are used to adjust the applied voltages on the electrodes. In particular, ω_p is changed by $2\delta\omega_2$ so that the parametric drive frequency coincides with ω_2. $V_{R,1}$ is also adjusted to account for the small difference between $\delta\omega_1$ and $\delta\omega_2$ so that $\Delta\omega \equiv \omega_2 - \omega_1$ is maintained at the desired value.

Voltage noise $V_{n,i}(t)$ is applied on the left electrode of resonator i to induce transitions between the two coexisting states of opposite phases. The noise voltage originates from the Johnson noise of a 50-Ω resistor at room temperature. After amplification, the noise voltage is bandpass filtered with center frequency $f_0 = 3000$ Hz and bandwidth $f_{\rm bd} = 40$ Hz. For resonator i, the filtered noise voltage is then mixed with a carrier voltage at frequency $f_{c,i}$ to generate two sidebands centered at $f_{c,i} \pm f_0$. For instance, in Fig. 3, f_{c1} and f_{c2} are 12841.8 Hz and 12851.8 Hz respectively. The resonant frequencies $\omega_{1,2}/2\pi$ lie within the corresponding upper sideband. The frequency difference $f_{c,2} - f_{c,1}$ is chosen to be much larger than the frequencies $\Gamma_i/2\pi$, $3\gamma_i A_i^2/2\pi\omega_p$ $(i = 1, 2)$ that characterize the motion of the modes in the rotating frame (here A_i is the vibration amplitude), so that the two resonators are effectively subjected to independent noise voltages, because the relevant spectral components originate from different frequencies of the pass band (note that the above characteristic frequencies are much smaller than 40 Hz). Finally, the noise voltages are multiplied by a factor c_i proportional to $\sqrt{\Gamma_i}/\Delta V_{L,i}$ to give $V_{n,i}(t)$ so that the effective temperature is identical in the two resonators. In Eq. (1), $\xi_i(t) = \frac{1}{M_i} C_i' \Delta V_{L,i} V_{n,i}(t)$ and the noise correlation time is $\sim 2\pi/f_{\rm bd}$. Therefore on the time scale of slow motion in the rotating frame the noise is effectively δ correlated.

APPENDIX C: MEASUREMENT OF SWITCHING RATES

To measure the switching rate of an individual resonator, its oscillation phase φ is recorded as a function of time using a lock-in amplifier. Figure 2(a) shows part of a record for resonator 1. If the resonator initially resides in the state $\sigma = -1$ with $\varphi \approx \pi$, we identify that it has switched to the $\sigma = +1$ state with $\varphi \approx 0$ when the phase goes over the threshold ε, where $\pi/4 < \varepsilon < \pi/2$. In switching from the initial state $\sigma = +1$ with $\varphi \approx 0$ the phase with overwhelming probability jumps to $-\pi \equiv \pi (\mathrm{mod} 2\pi)$. In this case the threshold is $-\pi + \varepsilon$. As the resonator switches back and forth between the two states, we record two sequences of residence times for the two states separately. The residence times in each state are plotted as a histogram. A typical histogram is shown in Fig. 6. The exponential decrease in the histogram confirms that the transitions are random and uncorrelated in time. An exponential fit to the histograms yields the switching rate. Fitting to a separate histogram gives the rate of switching from another state. We check that the measured switching rate does not depend on the choice of ε. For example, in Fig. 2(a), the dark and light lines indicate two different choices of threshold ε. They yield measured switching rates that are equal within the error bar of the fitting.

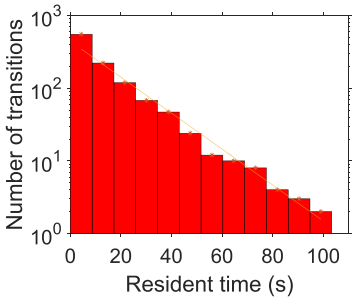

FIG. 6. Histogram of the residence times recorded for resonator 1 switching out of the $\sigma_1 = +1$ state at $F_d = 0$, $D = 3.01 \times 10^{-6}$ N^2 kg^{-2} Hz^{-1} and $\omega_p/2 = \omega_1$. The slope of the linear fit gives the rate of switching out of this state.

For uncoupled oscillators in the absence of the symmetry breaking drive, the measured switching rates out of the two states of each resonator are identical to within experimental uncertainty. Their value gives $\bar{W}_i$ for resonator i. Moreover, the stationary probability distributions $w_{\rm st}(\uparrow\downarrow)$, $w_{\rm st}(\downarrow\uparrow)$, $w_{\rm st}(\uparrow\uparrow)$, and $w_{\rm st}(\downarrow\downarrow)$ are measured to be equal to within measurement uncertainty (Appendix D).

To measure the logarithmic susceptibility of a single resonator, the switching rates are measured after the symmetry breaking drive is turned on. The fractional change of the switching rates for the two states are opposite in sign, as illustrated for resonator 1 in Fig. 2(c).

Logarithmic susceptibility can be calculated using the method of optimal fluctuation [42] or found from simulations [47]. The results have been established to be in excellent agreement. Therefore here we directly used simulations to find the magnitude χ and the phase δ of the logarithmic susceptibility. To do this we incorporated the drive $F_d \cos(\omega_p t/2 + \phi_d)$ into the equation of motion (1) of resonator 1 and set the coupling parameters V_{ij} equal to zero. We then switched to the rotating frame and used the standard rotating wave approximation to reduce the problem to a set of equations for the quadratures of $q_1(t)$. Forced vibrations at frequency $\omega_p/2$ in the laboratory frame correspond to stable stationary solutions of the equations for the quadratures in the absence of noise. Noise causes switching between these states. The residence times are identified and used to calculate the switching rate in a manner similar to the measurement procedure described above. This procedure allowed us to avoid simulating multiple ($\gtrsim 10^7 - 10^9$ in our case) oscillations of the parametric oscillator in the laboratory frame.

To measure the Ising model parameters K_{12} and K_{21}, the switching rates are measured before and after the coupling is turned on. The fractional change of the switching rates for resonators 1 and 2 are plotted in red and blue respectively in Fig. 3(c).

APPENDIX D: FLUCTUATIONS OF THE UNCOUPLED RESONATORS

For two uncoupled resonators ($V_{\rm cpl} = 0$ V), the stationary state populations $w_{st}(\uparrow\uparrow)$, $w_{st}(\downarrow\downarrow)$, $w_{st}(\uparrow\downarrow)$, and $w_{st}(\downarrow\uparrow)$ are measured to be near identical (Fig. 7). As shown in Fig. 7(b),

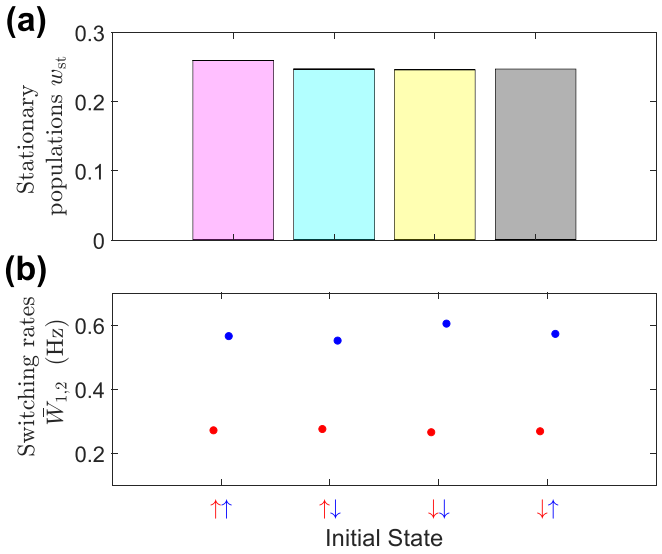

FIG. 7. (a) Stationary populations of the four states of two uncoupled resonators. (b) Measured rates of switching out of the states. For the red (blue) circles, only resonator 1 (2) switches.

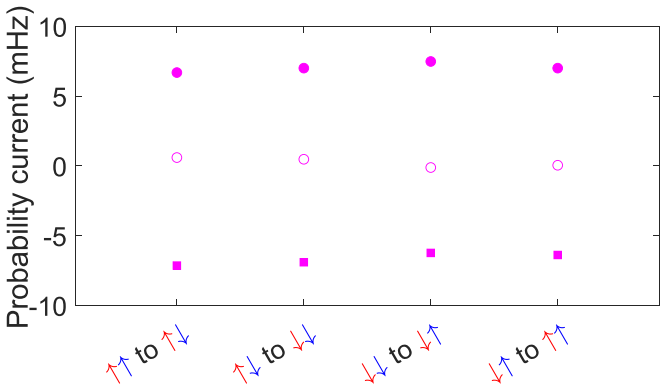

FIG. 8. The net probability current for each of the four pairs of transitions in the opposite directions for two coupled resonators for $\Delta\omega = -0.4$ Hz (solid squares), 0 Hz (hollow circles) and 0.4 Hz (solid circles).

the rates of switching for resonator 1, $\bar{W}_1(\sigma_1, \sigma_2 \to -\sigma_1, \sigma_2)$, are identical for all initial states to within measurement uncertainty. The measured switching rates for resonator 2, $\bar{W}_2(\sigma_1, \sigma_2 \to \sigma_1, -\sigma_2)$, are also identical for all states. However, the switching rates of different resonators are different: $\bar{W}_2(\sigma_1, \sigma_2 \to \sigma_1, -\sigma_2)$ exceeds $\bar{W}_1(\sigma_1, \sigma_2 \to -\sigma_1, \sigma_2)$ by a factor of ~ 2 because the resonators have slightly different damping constants.

APPENDIX E: MEASUREMENT OF PROBABILITY CURRENT

For two coupled resonators, there are eight transitions as shown in Fig. 3(b). In the experiment, we measure the switching rate for each transition as well as the stationary populations of the four states. The probability current from one state A to another state B is obtained using the following procedure. First, we evaluate the product of the measured stationary population of state A and the measured transition rate out of state A to state B. Then, we calculate the product of the measured stationary population of state B and the measured transition rate out of state B to state A. In general, these two products are not equal to each other. The net probability current from state A to state B is the difference between these two products. We find that the net probability currents for the four pairs of states are identical to within measurement uncertainty, as shown in Fig. 8 for three different values of $\Delta\omega$. This result is in agreement with Eq. (14). The values of the probability current plotted in Fig. 4 represents the mean value of the measured probability current for the four pairs of states in Fig. 8 for $\Delta\omega = -0.4$ Hz.

APPENDIX F: CHANGES OF ACTIVATION BARRIER BEYOND THE LINEAR REGIME

The effect of the coupling on the switching rate was seen in Ref. [14], but the logarithmic-susceptibility regime was not identified there. We emphasize that the mapping on the asymmetric Ising model in our study applies in the regime where the change of the activation barrier has the form $\Delta R_i(\sigma_i, \{\sigma_{j\neq i}\}) = D_i\sigma_i \sum_{j\neq i} K_{ij}\sigma_j$. In particular, for two oscillators $\Delta R_i(\sigma_i, \sigma_j) = -\Delta R_i(-\sigma_i, \sigma_j) = -\Delta R_i(\sigma_i, -\sigma_j)$. The value of $\Delta R_i(\sigma_i, \sigma_j)$ in this regime is determined by the logarithmic susceptibility, and in our experiment we have measured it independently.

The logarithmic-susceptibility regime refers to weak coupling. If the coupling is stronger, even where it does not lead to the onset of new vibrational states, not only are the switching rates modified, but the very stable states of individual oscillators, i.e., their amplitudes and phases, significantly change depending on the states of other oscillators. Therefore one cannot think of an oscillator as having just two states, which underlies the mapping on a spin system.

When the amplitude F_d of the symmetry-breaking drive is small for an individual, uncoupled resonator, the change in the vibration amplitudes of the two states is also small. The changes of the activation barriers $\Delta R_i(\sigma_i = +1)$ and $\Delta R_i(\sigma_i = -1)$ are of opposite signs but near identical magnitude. $|\Delta R_i|$ is proportional to the amplitude of the symmetry breaking drive, with a proportionality constant given by the logarithmic susceptibility. As F_d increases, the difference in the vibration amplitudes and phases of the two states cannot be ignored. Figure 9(a) extends the range of F_d of Fig. 2(d) to show that, for resonator 1, $|\Delta R_1(\sigma_1 = +1)|$ and $|\Delta R_1(\sigma_1 = -1)|$ are no longer equal for large F_d. Furthermore, the dependence of $\Delta R_1(\sigma_1)$ on F_d does not follow a linear relationship. Figure 9(b) shows a similar plot for resonator 2.

As described in Sec. IV, when weak coupling is turned on between two resonators, the effects on resonator 1 from the coupling to resonator 2 can be understood in terms of the logarithmic susceptibility of resonator 1 subjected to a symmetry breaking drive, and vice versa for resonator 2. Beyond the weak coupling regime, the increase in switching rates for initial states with identical phases is no longer equal in magnitude to the decrease of switching rates for initial states with opposite phases. In fact, the phase difference between the two vibration states in each oscillator deviates considerably from π. Figure 10 shows the measured and simulated results

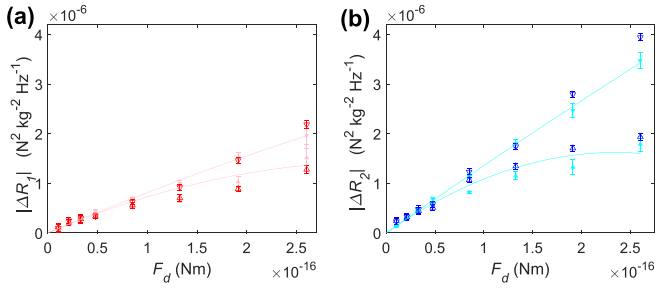

FIG. 9. (a) Increments $|\Delta R_1(\sigma_1 = +1)|$ (up triangles) and $|\Delta R_1(\sigma_1 = -1)|$ (down triangles) of the activation energy as a function of F_d for resonator 1. The range of F_d is about 5 times larger than in Fig. 2(d). Measurements and numerical simulations are shown in red and pink respectively. The lines are fits to the simulated results by parabola. They have the same linear term as the line in Fig. 2(d). Different quadratic terms are used for $\sigma_1 = \pm 1$. (b) Similar plot for resonator 2. Measurements and numerical simulations are shown in dark blue and light blue respectively.

for the change of the activation barrier when the range of $V_{\rm cpl}$ is extended beyond that in Fig. 3(d). While Fig. 3(d) plots $|\Delta R_{1,2}|$, Figs. 10(a) and 10(b) show $\Delta R_1(\sigma_1, \sigma_2)$ and $\Delta R_2(\sigma_1, \sigma_2)$ separately and without the absolute value. Since $W_i(\sigma_i, \sigma_j) = W_i(-\sigma_i, -\sigma_j)$ as described by Eq. (8), it follows that $\Delta R_i(\sigma_i, \sigma_j) = \Delta R_i(-\sigma_i, -\sigma_j)$. In Fig. 10, the up triangles represent the average of the measured values of $\Delta R_i(\uparrow\downarrow)$ and $\Delta R_i(\downarrow\uparrow)$. The down triangles represent the average of $\Delta R_i(\uparrow\uparrow)$ and $\Delta R_i(\downarrow\downarrow)$, both of which are negative. The results for Fig. 3(d) are obtained by averaging $|\Delta R_i(\uparrow\downarrow)|$, $|\Delta R_i(\downarrow\uparrow)|$, $|\Delta R_i(\uparrow\uparrow)|$, and $|\Delta R_i(\downarrow\downarrow)|$ for $V_{\rm cpl}^2 < 0.1$ V^2. For $V_{\rm cpl}^2 > 0.1$ V^2, the difference in the magnitude of $\Delta R_{1,2}$ for initial states of the same and opposite phases becomes more apparent. In Figs. 10(a) and 10(b), the sum of the top and bottom branches are shown as the thick lines, the deviation of which from zero increases with $V_{\rm cpl}^2$.

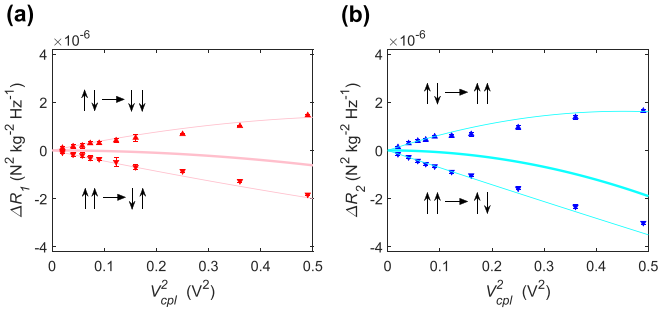

FIG. 10. (a) Dependence of the change ΔR_1 of activation barriers for switching of resonator 1 on $V_{\rm cpl}^2$. Initial states with the phase of resonator 1 identical (opposite) to resonator 2 are represented by up triangles (down triangles). Measurements are shown in red. The thin pink lines are obtained from theory based on the effect of a symmetry breaking drive on individual uncoupled resonators using numerical simulations from Fig. 9. The thick pink line is a sum of the thin lines. (b) Similar plot for resonator 2. Measurements and numerical simulations are shown in blue and light blue respectively.

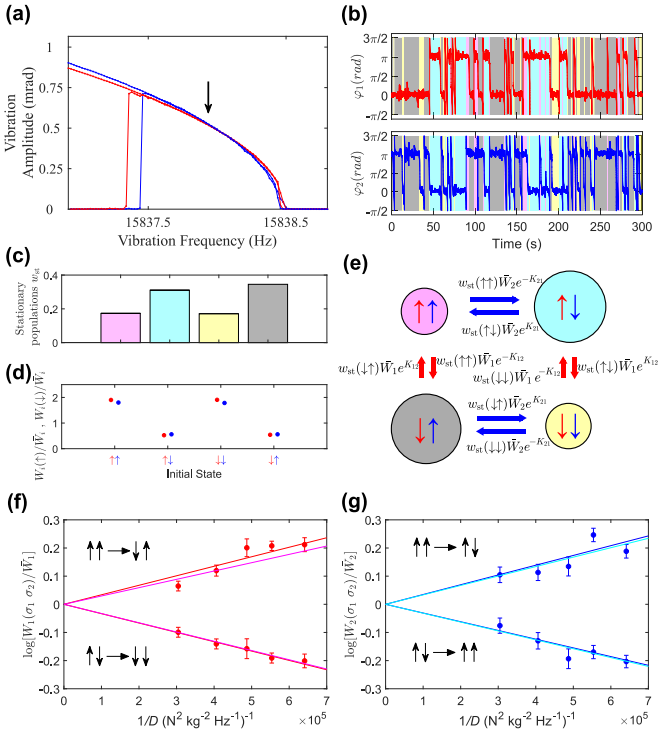

FIG. 11. (a) Vibration amplitudes of resonator 1 (red) and 2 (blue), with $\Delta\omega/2\pi = 0$ Hz and $V_{\rm cpl} = 0.3$ V, under identical parametric modulation with no noise added. (b) Typical records of the phase of the two resonators as a function of time when noise is added. (c) Stationary probability distributions of the four states. (d) Change of the transition rates from the four initial states due to coupling. For red (blue) circles, only resonator 1 (2) switches. (e) Switchings between the four states. The areas of circles are proportional to the measured stationary probability distributions $w_{st}(\sigma_1, \sigma_2)$. The lengths of the arrows are proportional to the product of the measured switching rates and the corresponding initial stationary probability distribution. (f) Logarithm of the measured changes of the transition rates due to coupling as a function of $1/D$ for resonator 1. The magnitude of the slopes of the linear fits yields $|\Delta R_1|$. (g) Similar plot for resonator 2, with $|\Delta R_2|$ given by the magnitude of the slope of the linear fit.

APPENDIX G: POPULATION AND TRANSITION RATES OF COUPLED IDENTICAL RESONATORS

In this section, we tune the difference between K_{12} and K_{21} to near zero by choosing $\Delta\omega/2\pi = 0$ Hz. As a result, the probability current vanishes to within experimental uncertainty. Detailed balance is restored and our system maps onto the symmetric Ising model.

Figure 11(a) shows the vibration amplitudes of the two resonators with $\Delta\omega/2\pi = 0$ Hz under parametric modulation in the absence of injected noise. The slight difference between the response curves is due to the difference in the decay rates of the modes. Application of noise leads to switching in both resonators, as illustrated in Fig. 9(b). As a result of the coupling ($V_{\rm cpl} = 0.3$ V) that favors opposite phases in the two resonators, the transition rates $W_i(\sigma_i, \{\sigma_j = \sigma_i\})$ and $W_i(\sigma_i, \{\sigma_j = -\sigma_i\})$ are increased and decreased compared to the uncoupled values $\bar{W}_i$ respectively. Moreover, the fractional changes for resonators 1 and 2 are identical to within exper-

imental uncertainty, as shown by the adjacent red and blue circles in Fig. 11(d). Figures 11(f) and 11(g) plot the change in transition rates due to the coupling as a function of $1/D$ for resonators 1 and 2 respectively. The magnitudes of the slopes of the linear fits are identical to within ∼10% consistent with $|\Delta R_1| = |\Delta R_2|$ and hence $K_{12} = K_{21} = K$.

We examine how detailed balance is manifested in the probability current, taking the transitions between the ↑↑ state and ↑↓ state as an example. The transition rates $W_1(\uparrow\uparrow)$ and $W_1(\uparrow\downarrow)$ are changed from $\bar{W}_1$ by factors $\exp(-K)$ and $\exp(K)$ respectively. The stationary probability distribution for $K_{ij} = K_{ji} = K$ is $w_{st} = Z^{-1}\exp[\frac{1}{2}\sum_{i,j(i\neq j)} K\sigma_i\sigma_j]$ where Z is the normalization factor. In the case of two resonators we see that $w_{st}(\uparrow\uparrow)$ and $w_{st}(\uparrow\downarrow)$ are changed from their value $\frac{1}{4}$ in the absence of coupling by $Z^{-1}\exp(K)$ and $Z^{-1}\exp(-K)$ respectively, where $Z = 4\cosh K$ [Fig. 11(c)]. The products $W_1(\uparrow\uparrow)w_{st}(\uparrow\uparrow)$ and $W_1(\uparrow\downarrow)w_{st}(\uparrow\downarrow)$ remain equal in magnitude, as represented by the same length of the two block arrows in Fig. 11(e). The net probability current between the states ↑↑ and ↑↓ is therefore zero.

APPENDIX H: WEAKLY ASYMMETRIC CHAIN

To illustrate the nontrivial effect of the asymmetry on the stationary distribution we briefly consider the case where the asymmetry is weak,

$$K_{ij} = \bar{K}_{ij} + \delta K_{ij}, \quad \bar{K}_{ij} = \bar{K}_{ji}, \quad \delta K_{ij} = -\delta K_{ji}, \tag{H1}$$

with $|\delta K_{ij}| \ll |\bar{K}_{ij}|$. To zeroth order in δK_{ij}, the stationary distribution $w_{\rm st}^{(0)}$ is given by the standard Ising-model expression

$$w_{\rm st}^{(0)} = Z^{-1}\exp\left(\frac{1}{2}\sum_{i,j}\bar{K}_{ij}\sigma_i\sigma_j\right),$$

where Z is an equivalent of the partition function.

To reveal the complexity of the dynamics we can further simplify the analysis by considering nearest-neighbor coupling, $\bar{K}_{ij} = \bar{K}\delta_{i\,j\pm1}$, and assuming that the rates $\bar{W}_i$ are the same for all spins, $\bar{W}_i = \bar{W}, \forall i$. We will seek the first-order correction to the stationary distribution in the form $w_{\rm st}^{(0)}(\{\sigma_i\})w_{\rm st}^{(1)}(\{\sigma_i\})$. This correction is given by a set of equations

$$\begin{aligned}\bar{W}\,w_{\rm st}^{(0)}&\sum_{i=1}^{N}\exp[-\bar{K}\sigma_i(\sigma_{i+1}+\sigma_{i-1})]\\ &\times\left[w_{\rm st}^{(1)}(\sigma_i,\{\sigma_{j\neq i}\}) - w_{\rm st}^{(1)}(-\sigma_i,\{\sigma_{j\neq i}\})\right]\\ &= -2\bar{W}\,w_{\rm st}^{(0)}\sinh\bar{K}\sum_{i=1}^{N}\exp(-\bar{K}\sigma_i\sigma_{i+1})\\ &\times\delta K_{i\,i+1}(\sigma_{i-1}\sigma_{i+1}-\sigma_i\sigma_{i+2}).\end{aligned} \tag{H2}$$

The equation set (H2) for 2^{N-1} independent components of $w_{\rm st}^{(1)}(\{\sigma_i\})$ (on account of the symmetry $\{\sigma_i\}\to\{-\sigma_i\}$) has actually only $2^{N-1}-1$ independent equations and needs to be complemented by the condition $\sum_{\{\sigma_i\}} w_{\rm st}^{(0)}(\{\sigma_i\})\times w_{\rm st}^{(1)}(\{\sigma_i\}) = 0$.

It immediately follows from Eq. (H2) that the correction $w_{\rm st}^{(1)}$ to the stationary distribution, even though linear in δK_{ij}, is "nonlocal", as each term in the sum over i in the right-hand side depends on spins on four sites. Therefore this correction describes the modification of extended correlations in the system by the asymmetry.

We note that for $N = 2$ the right-hand side of Eq. (H2) is zero. In this case there is no first-order correction to the stationary distribution. This is seen from the explicit form of $w_{\rm st}$ in the main text. However, already for $N = 3$, one can see from Eq. (H2) that all probabilities $w_{\rm st}^{(1)}(\{\sigma_i\})$ are affected by δK_{ij}.

We note also that the difference of the left- and right-hand sides of Eq. (H2) can be written as the sum of the site currents $\sum_i I(\sigma_i,\{\sigma_{j\neq i}\}\to-\sigma_i,\{\sigma_{j\neq i}\})$. The current on each site is nonzero already in the first order in the asymmetry δK_{ij}, but the sum of the currents over the sites is equal to zero. This is the analog of the Kirchhoff law for the probability current in the stationary regime.

[1] L. D. Landau and E. M. Lifshitz, *Mechanics*, 3rd ed. (Elsevier, Amsterdam, 2004).

[2] E. Goto, The parametron, a digital computing element which utilizes parametric oscillation, Proc. IRE **47**, 1304 (1959).

[3] I. Mahboob and H. Yamaguchi, Bit storage and bit flip operations in an electromechanical oscillator, Nat. Nanotechnol. **3**, 275 (2008).

[4] Z. Leghtas, S. Touzard, I. M. Pop, A. Kou, B. Vlastakis, A. Petrenko, K. M. Sliwa, A. Narla, S. Shankar, M. J. Hatridge *et al.*, Confining the state of light to a quantum manifold by engineered two-photon loss, Science **347**, 853 (2015).

[5] A. Grimm, N. E. Frattini, S. Puri, S. O. Mundhada, S. Touzard, M. Mirrahimi, S. M. Girvin, S. Shankar, and M. H. Devoret, Stabilization and operation of a Kerr-cat qubit, Nature (London) **584**, 205 (2020).

[6] Z. Wang, A. Marandi, K. Wen, R. L. Byer, and Y. Yamamoto, Coherent Ising machine based on degenerate optical parametric oscillators, Phys. Rev. A **88**, 063853 (2013).

[7] P. L. McMahon, A. Marandi, Y. Haribara, R. Hamerly, C. Langrock, S. Tamate, T. Inagaki, H. Takesue, S. Utsunomiya, K. Aihara *et al.*, A fully programmable 100-spin coherent Ising machine with all-to-all connections, Science **354**, 614 (2016).

[8] H. Goto, Bifurcation-based adiabatic quantum computation with a nonlinear oscillator network, Sci. Rep. **6**, 21686 (2016).

[9] S. Puri, Ch. K. Andersen, A. L. Grimsmo, and A. Blais, Quantum annealing with all-to-all connected nonlinear oscillators, Nat. Commun. **8**, 15785 (2017).

[10] H. Goto, Z. Lin, and Y. Nakamura, Boltzmann sampling from the Ising model using quantum heating of coupled nonlinear oscillators, Sci. Rep. **8**, 7154 (2018).

[11] L. Bello, M. Calvanese Strinati, E. G. Dalla Torre, and A. Pe'er, Persistent coherent beating in coupled parametric oscillators, Phys. Rev. Lett. **123**, 083901 (2019).

[12] Y. Yamamoto, T. Leleu, S. Ganguli, and H. Mabuchi, Coherent Ising machines—Quantum optics and neural network perspectives, Appl. Phys. Lett. **117**, 160501 (2020).

[13] T. L. Heugel, O. Zilberberg, C. Marty, R. Chitra, and A. Eichler, Ising machines with strong bilinear coupling, Phys. Rev. Res. **4**, 013149 (2022).

[14] P. Álvarez, D. Pittilini, F. Miserocchi, S. Raamamurthy, G. Margiani, O. Ameye, J. del Pino, O. Zilberberg, and A. Eichler, A biased Ising model using two coupled Kerr parametric oscillators with external force, arXiv:2307.13676.

[15] D. Rugar and P. Grütter, Mechanical parametric amplification and thermomechanical noise squeezing, Phys. Rev. Lett. **67**, 699 (1991).

[16] R. B. Karabalin, R. Lifshitz, M. C. Cross, M. H. Matheny, S. C. Masmanidis, and M. L. Roukes, Signal amplification by sensitive control of bifurcation topology, Phys. Rev. Lett. **106**, 094102 (2011).

[17] M. I. Dykman, C. M. Maloney, V. N. Smelyanskiy, and M. Silverstein, Fluctuational phase-flip transitions in parametrically driven oscillators, Phys. Rev. E **57**, 5202 (1998).

[18] L. J. Lapidus, D. Enzer, and G. Gabrielse, Stochastic phase switching of a parametrically driven electron in a penning trap, Phys. Rev. Lett. **83**, 899 (1999).

[19] M. Marthaler and M. I. Dykman, Switching via quantum activation: A parametrically modulated oscillator, Phys. Rev. A **73**, 042108 (2006).

[20] H. B. Chan and C. Stambaugh, Activation barrier scaling and crossover for noise-induced switching in micromechanical parametric oscillators, Phys. Rev. Lett. **99**, 060601 (2007).

[21] H. B. Chan, M. I. Dykman, and C. Stambaugh, Paths of fluctuation induced switching, Phys. Rev. Lett. **100**, 130602 (2008).

[22] J. Venkatraman, R. G. Cortinas, N. E. Frattini, X. Xiao, and M. H. Devoret, Quantum interference of tunneling paths under a double-well barrier, arXiv:2211.04605.

[23] K. Kim, M. S. Heo, K. H. Lee, K. Jang, H. R. Noh, D. Kim, and W. Jhe, Spontaneous symmetry breaking of population in a nonadiabatically driven atomic trap: An Ising-class phase transition, Phys. Rev. Lett. **96**, 150601 (2006); M. S. Heo, Y. Kim, K. Kim, G. Moon, J. Lee, H. R. Noh, M. I. Dykman, and W. Jhe, Ideal mean-field transition in a modulated cold atom system, Phys. Rev. E **82**, 031134 (2010).

[24] M. I. Dykman, C. Bruder, N. Lörch, and Y. Zhang, Interaction-induced time-symmetry breaking in driven quantum oscillators, Phys. Rev. B **98**, 195444 (2018).

[25] T. L. Heugel, M. Oscity, A. Eichler, O. Zilberberg, and R. Chitra, Classical many-body time crystals, Phys. Rev. Lett. **123**, 124301 (2019).

[26] A. J. Kollár, M. Fitzpatrick, and A. A. Houck, Hyperbolic lattices in circuit quantum electrodynamics, Nature (London) **571**, 45 (2019).

[27] N. Carlon Zambon, S. R. K. Rodriguez, A. Lemaitre, A. Harouri, L. Le Gratiet, I. Sagnes, P. St-Jean, S. Ravets, A. Amo, and J. Bloch, Parametric instability in coupled nonlinear microcavities, Phys. Rev. A **102**, 023526 (2020).

[28] J. J. Hopfield, Neural networks and physical systems with emergent collective computational abilities., Proc. Natl. Acad. Sci. USA **79**, 2554 (1982).

[29] D. Krotov, A new frontier for Hopfield networks, Nat. Rev. Phys. **5**, 366 (2023).

[30] C. Lucibello and M. Mézard, Exponential capacity of dense associative memories, Phys. Rev. Lett. **132**, 077301 (2024).

[31] H. Sompolinsky and I. Kanter, Temporal association in asymmetric neural networks, Phys. Rev. Lett. **57**, 2861 (1986).

[32] G. Parisi, Asymmetric neural networks and the process of learning, J. Phys. A: Math. Gen. **19**, L675 (1986).

[33] B. Derrida, E. Gardner, and A. Zippelius, An exactly solvable asymmetric neural network model, Europhys. Lett. **4**, 167 (1987).

[34] M. Mézard and J. Sakellariou, Exact mean-field inference in asymmetric kinetic Ising systems, J. Stat. Mech. (2011) L07001.

[35] H. Huang and Y. Kabashima, Dynamics of asymmetric kinetic Ising systems revisited, J. Stat. Mech. (2014) P05020.

[36] M. Aguilera, S. A. Moosavi, and H. Shimazaki, A unifying framework for mean-field theories of asymmetric kinetic Ising systems, Nat. Commun. **12**, 1197 (2021).

[37] A. Szedlak, G. Paternostro, and C. Piermarocchi, Control of asymmetric Hopfield networks and application to cancer attractors, PLoS ONE **9**, e105842 (2014).

[38] S. Cocco, S. Leibler, and R. Monasson, Neuronal couplings between retinal ganglion cells inferred by efficient inverse statistical physics methods, Proc. Natl. Acad. Sci. USA **106**, 14058 (2009).

[39] A. J. Mendoza and J. S. Haas, Intrinsic sources and functional impacts of asymmetry at electrical synapses, eNeuro **9**, ENEURO.0469-21.2022 (2022).

[40] M. Fruchart, R. Hanai, P. B. Littlewood, and V. Vitelli, Nonreciprocal phase transitions, Nature (London) **592**, 363 (2021).

[41] R. J. Glauber, Time-dependent statistics of the Ising model, J. Math. Phys. **4**, 294 (1963).

[42] V. N. Smelyanskiy, M. I. Dykman, H. Rabitz, and B. E. Vugmeister, Fluctuations, escape, and nucleation in driven systems: Logarithmic susceptibility, Phys. Rev. Lett. **79**, 3113 (1997).

[43] H. Kramers, Brownian motion in a field of force and the diffusion model of chemical reactions, Phys. Utrecht **7**, 284 (1940).

[44] D. G. Luchinsky, R. S. Maier, R. Mannella, P. V. E. McClintock, and D. L. Stein, Observation of saddle-point avoidance in noise-induced escape, Phys. Rev. Lett. **82**, 1806 (1999).

[45] D. Ryvkine and M. I. Dykman, Resonant symmetry lifting in a parametrically modulated oscillator, Phys. Rev. E **74**, 061118 (2006).

[46] I. Mahboob, C. Froitier, and H. Yamaguchi, A symmetry-breaking electromechanical detector, Appl. Phys. Lett. **96**, 213103 (2010).

[47] D. G. Luchinsky, R. Mannella, P. V. E. McClintock, M. I. Dykman, and V. N. Smelyanskiy, Thermally activated escape of driven systems: The activation energy, J. Phys. A: Math. Gen. **32**, L321 (1999).

[48] M. H. Devoret, D. Esteve, J. M. Martinis, A. Cleland, and J. Clarke, Resonant activation of a Brownian particle out of a potential well: Microwave-enhanced escape from the zero-voltage state of a Josephson junction, Phys. Rev. B **36**, 58 (1987).